Chemical Composition in the Globular Cluster M71 from Keck/HIRES Spectra of Turn-Off Stars

Ann Merchant Boesgaard[1]

Institute for Astronomy, University of Hawai'i at Manoa
2680 Woodlawn Drive, Honolulu, HI 96822-1839

boes@ifa.hawaii.edu

Jeremy R. King[1]

Department of Physics and Astronomy, 118 Kinard Laboratory,
Clemson University, Clemson, SC 29634

jking2@ces.clemson.edu

Ann Marie Cody

Department of Astronomy Option
California Institute of Technology, MS 105-24, Pasadena, CA 91125

amc@astro.caltech.edu

Alex Stephens[1]

Institute for Astronomy, University of Hawai'i at Manoa
2680 Woodlawn Drive, Honolulu, HI 96822-1839

alex_c_stephens@yahoo.com

Constantine P. Deliyannis[1]

Department of Astronomy, Indiana University
727 East 3rd Street, Swain Hall West 319, Bloomington, IN 47405-7105

con@athena.astro.indiana.edu

ABSTRACT

[1]Visiting Astronomer, W. M. Keck Observatory, jointly operated by the California Institute of Technology and the University of California.

We have made observations with the Keck I telescope and HIRES at a resolution of ∼45,000 of five nearly identical stars at the turn-off of the metal-rich globular cluster M 71. We derive stellar parameters and abundances of several elements. Our mean Fe abundance, [Fe/H]= -0.80 ± 0.02, is in excellent agreement with previous cluster determinations from both giants and near-turnoff stars. There is no clear evidence for any star-to-star abundance differences or correlations in our sample. Abundance ratios of the Fe-peak elements (Cr, Ni) are similar to Fe. The turn-off stars in M71 have remarkably consistent enhancements of 0.2 - 0.3 dex in [Si/Fe], [Ca/Fe] and [Ti/Fe] – like the red giants. Our [Mg/Fe] ratio is somewhat lower than that suggested by other studies. We compare our mean abundances for the five M 71 stars with field stars of similar metallicity [Fe/H] – 8 with halo kinematics and 17 with disk kinematics. The abundances of the alpha-fusion products (Mg, Si, Ca, Ti) agree with both samples, but seem a closer match to the disk stars. The Mg abundance in M71 is at the lower edge of the disk and halo samples. The neutron-capture elements, Y and Ba, are enhanced relative to solar in the M71 turn-off stars. Our ratio [Ba/Fe] is similar to that of the halo field stars but a factor of two above that for the disk field stars. The important [Ba/Y] ratio is significantly lower than M71 giant values; the pre-cluster material may have been exposed to a higher neutron flux than the disk stars or self-enrichment has occured subsequent to cluster star formation. The Na content of the M71 turn-off stars is remarkably similar to that in the disk field stars, but more than a factor of two higher than the halo field star sample. We find [Na/Fe] = $+0.14\ \pm0.04$ with a spread less than half of that found in the red giants in M71. Excluding Mg, the lack of intracluster α-element variations (turn-off vis-a-vis giants) suggests the polluting material needed to explain the abundance patterns in M71 did not arise from explosive nucleosynthesis, but arose in a more traditional s-process environment such as AGB stars. The determination of light s-peak abundances should reveal whether this pollution occurred before or after cluster formation.

Subject headings: stars: abundances; globular clusters: abundances; globular clusters: individual (M 71)

1. INTRODUCTION

It is important to determine the composition of unevolved stars in globular clusters in order to learn the basic composition of the cluster from stars that have not undergone

any mixing with the interior layers. We include as "unevolved stars" both main sequence and turn-off stars. It is well known that there can be large spreads in the abundance of some elements in the giant stars of a given globular cluster (e.g. Kraft 1994, Sneden et al. 1997). Most previous high-resolution studies were limited to giant stars, whose atmospheres and interiors are less well modeled than those of dwarf stars. More extensive studies of the unevolved stars, which have little or no advanced nuclear processing *in situ*, are expected to reveal the clusters' original composition.

It now seems clear that mixing and evolutionary effects in cluster giants mean that these stars cannot be used to probe the original abundance patterns in clusters. The the light elements (e.g. C, N, O, Na, Al) in the giants evince rich intra-cluster differences that makes it impossible to ascertain a universal pattern of light element alterations. Good evidence exists, e.g., that CNO cycling and NeNa/MgAl burning in M13 has a considerable *in situ* component (Pilachowski et al. 1996; Briley & Cohen 2001). Conventional wisdom now holds that such abundance modifications can be explained by a combination of p-capture reactions (Denisenkov & Denisenkova 1990; Langer, Hoffman & Sneden 1993) and some non-standard deep mixing mechanism (Cavallo, Sweigart & Bell 1996) perhaps operating particularly more efficiently in low metallicity clusters owing to smaller stellar interior mean molecular weight gradients. The most direct means, however, to explore *in situ* versus primordial (or self-enrichment) mechanisms is to determine the composition of unevolved stars in globular clusters. More extensive studies of the unevolved stars, which have little or no advanced nuclear processing *in situ*, are expected to provide a baseline of clusters' red giants' original composition(s) onto which the additions - by other mechanisms - are made.

Several groups have begun studying globular cluster stars over a range of evolutionary stages, including turn-off stars at high spectral-resolution (e.g. Gratton et al. 2001; Cohen & Meléndez 2005). These initial efforts, and previous photometric and low-resolution spectroscopic results, have revealed strong evidence that some light element abundance alterations in some clusters are present prior to reaching the red giant branch, thus suggesting the possibilities of primordial variations, self-enrichment mechanisms, or totally unexpected mixing mechanisms. Briley et al. (1994) found anti-correlated CN and CH band strength variations at the turnoff of 47 Tuc, and suggested that this cluster's CN distribution changes little with evolutionary status; additionally striking is the existence of Na abundance variations on the 47 Tuc main-sequence reported by Briley et al. (1996). Utilizing Keck data, Briley & Cohen (2001) find that CNO abundances in M71 show little evolution from the main-sequence to bright giants; moreover, the bimodal and anti-correlated CN and CH distributions of M71 red giants are found to be in place on the main-sequence. Gratton et al. (2001) find that an O-Na (and Mg-Al and C-N) anticorrelation, previously seen only in globular red giants, exists in turn-off stars in NGC 6752. Ramírez & Cohen (2002) (hereafter RC02) utilized

high-resolution Keck/HIRES data to find that an O-Na anticorrelation exists in M71 from its turnoff to giants above the red HB level. For an excellent review of globular cluster abundances and abundance variations, see Gratton, Sneden & Carretta (2004).

We have embarked on a high spectral-resolution study of turn-off stars in a number of globular clusters. Such stars are faint, so to observe them at high resolution requires long integration times on the largest telescopes. We have used the Keck I 10-m telescope with HIRES to make observations of $V\sim$18 turn-off stars in M92, M71, M13, and M5. Results on M92 have been published on Li in Boesgaard et al. (1998) and on Fe, Na, Mg, Ca, Ti, Cr and Ba in King et al. (1998). The latter paper found [Fe/H][2] $= -2.52$ for unevolved stars, compared to -2.25 for giants found by Sneden et al. (1991). The reason for the dwarf-giant difference remains unclear, but the homogeneous analyses of NGC 6397 and 6752 (Gratton et al. 2001) and M71 (Ramírez & Cohen 2001, RC02) indicate no difference in [Fe/H] values (or Fe peak, n-capture, and α-element abundances for the M71 cluster) between turnoff stars and more evolved cluster stars. King et al. (1998) also found large Mg depletions and Na enhancements compared to HD 140283, a mildly evolved halo subgiant with similar [Fe/H] and evolutionary state; [Ba/Fe] also appeared to be enhanced in the M92 stars compared to HD 140283. King et al. (1998) noted these qualitative patterns were reminiscent of those believed to be due to MgAl and NeNa cycling in red giants. (See the recent discussion by Aikawa et al. (2004) on the reaction rates in these chains related to observations in red giants in globular clusters.) Additionally, they dedicated considerable discussion to wrestling with the difficulty in understanding how such processing (whether *in situ* or from polluted material processed in a previous stellar generation) could co-exist without resulting in remarkably depleted Li abundances. Bonifacio et al. (2002) noted a similar "paradox" for NGC 6397, which appears to be analogous to that seen in the metal-poor field (Spite & Spite 1986). Bonifacio et al. (2002) mention preliminary evidence of prominent N enhancements in NGC 6397 subgiants, indicative of CN processing or supernovae in massive stars. If those enhancements are due to internal processing in their turnoff stars, then how does Li remain "normal"? Similarly, Thévenin et al. (2001) note that one of their NGC 6397 turn-off stars demonstrates a relative 0.4 dex Na deficiency; however, this star also evinces unremarkable Li.

This summary paints a complex and rich picture of globular cluster abundances–one that will probably only be understood on a cluster-by-cluster (if not star-by-star) basis. Here we present observations, analysis, and results from a study of five turn-off stars in M71. We have determined abundances for three iron-peak elements (Fe, Cr, and Ni), four

[2]We use the usual notation [Element/H] = log N(Element/H)$_{star}$/log N(Element/H)$_{\odot}$

alpha-fusion elements (Mg, Si, Ca, and Ti), two rare-earth elements (Y and Ba) and Na. The globular cluster M71 is especially interesting for this work because it is very old ($\geq$12 Gyr; Grundahl, Stetson & Andersen 2002), yet relatively metal-rich ([Fe/H]~ -0.8) for a globular cluster. Sneden et al. (1994) (hereafter SKLPS) find [Fe/H] = -0.79 from 10 red giants. Cohen, Behr & Briley (2001), Ramírez et al. (2001) and RC02 have reported on Keck/HIRES observations of M71 of stars of a variety of evolutionary stages including three stars near the turn-off.

The stars we observed in M71 have the same age, mass, luminosity, and temperature as each other and as the stars in M 92, but the two clusters differ in metallicity by a factor of $\sim$50. We have selected M 71 because 1) it is a little brighter than M 92 at the turnoff ($V = 17.7$ versus 18.0); 2) despite considerable reddening ($E(B-V)\sim0.28$), it has excellent photometry (Hodder et al. 1992); 3) it is a disk globular with relatively high metal content; 4) its space motion indicates that it is probably a member of the thick disk population (Cudworth & Hanson 1993).

We report on our four general goals: First, to characterize the abundances of relatively unevolved stars in M71. Second, to compare these with determinations from both other near-turnoff stars (RC02) and red giants (SKLPS, RC02) in M71. Third, to compare our M71 turn-off abundances with those in field halo stars and field disk stars of the same metallicity. Fourth, to search for evidence of photospheric material having suffered p-capture and deep mixing.

2. Observations and Data Reduction

Keck/HIRES spectral observations with respectable signal-to-noise (S/N) ratios of stars near V = 18 require exposures of several hours. However, individual intergration times did not exceed 45-60 minutes due to the contamination by "cosmic ray" events. On the other hand, the exposures needed to be long enough to obtain a high enough signal so that individual frames could be co-added reliably at the correct wavelength justification. In metal-poor stars where the spectral lines are weak this can be problematic. Therefore, we could only make these observations on cloudless nights with good seeing.

The spectra for this project were obtained at the Keck 10-m telescope with HIRES (Vogt et al. 1994) over three observing seasons on four observing runs comprising seven nights. The same settings (slit dimensions, echelle and cross-disperser angles, filters) were used on each run. Approximately 2400 Å were covered from 4430 – 6880 Å with some gaps between orders longward of 5000 Å. The positions in the color-magnitude diagram of our five stars can be

seen in Figure 1. The fiducial sequence is taken from Hodder et al. (1992).

The details of the observations for our five stars are shown in Table 1 which gives the dates of the observations and the details of the multiple exposures on multiple nights. The star identifications are those of Hodder et al. (1992). The photometric data for V and (B−V) are from Hodder et al. (1992) as is the assumed reddening correction of E(B−V) = 0.28. This value of the reddening agrees well with that of both Zinn (1980) of 0.27 ±0.03 and that of Geffert & Maintz (2000) of 0.27 ±0.05. The final column shows the signal-to-noise ratio of the combined spectra. As can be seen in Table 1, the integration times were 135 - 285 minutes to reach the listed S/N ratios (per pixel) of 50-60. We have also made use of a spectrum of the moon as a solar proxy that we obtained with the same settings on HIRES as our stellar spectra. The lunar spectrum was a 30 s exposure obtained on 29 July 1994 with a S/N ratio near 1400.

Standard data reduction procedures were carried out with IRAF[3] routines. Individual frames were trimmed, overscan-subtracted, and bias-subtracted (the median of numerous overscan-subtracted bias frames from each night). Typically 20 quartz flat-field exposures were obtained each night and these processed frames were combined to form a master nightly flat-field frame. Frames of the stars in M71 were pre-processed in the same fashion and then divided by a normalized flat field, which was produced by fitting a low order spline to the blaze+lamp function.

Scattered light was removed by fitting a low-order polynomial to the inter-order regions across the dispersion and smoothing them along the dispersion. Cosmic ray hits were removed interactively. Typically, 29 orders were identified, traced and extracted. The wavelength scale was found from the positions of many lines in each order of the Th-Ar comparison spectrum. The measured spectral resolution is ∼45,000. The dispersion-corrected, extracted 1-dimensional spectra were co-added order-by-order. The final spectrum of each star was then continuum normalized.

For most of the spectral analysis the individual orders were smoothed by a 3-pixel boxcar in order to increase the effective S/N ratio with minimal impact upon the spectral resolution. Examples of two spectral regions in the spectra for three of the stars are shown in Figures 2 and 3. Spectral features from several ions are identified in these figures. The three stars shown all have the same value of (B−V) and the line strengths are clearly similar in all three.

---

[3]IRAF is distributed by the National Optical Astronomical Observatories, which are operated by AURA, Inc. under contract to the NSF.

3. ABUNDANCE ANALYSIS

3.1. Line Measurements

We have made measurements of the equivalent widths of some 200 lines in each of our five stars and 117 in the sun/moon spread throughout the 29 orders of our Keck spectra. The relevant features include those of the: Fe-peak elements (Fe I and Fe II, Cr I and Cr II, and Ni I); alpha-fusion elements (Mg I, Si I and Si II, Ca I, and Ti I and Ti II); the alkali element Na (Na I); and the neutron-capture elements (Y II and Ba II). The splot package in IRAF was used to measure the equivalent widths via gaussian profile fitting. Lines that were noticeably blended were not used; thus, nearly all could be measured using both sides of the line profile. The measured equivalent widths ranged from 7 to 200 mÅ, but lines used for the parameter and abundance determinations were typically $\leq$80 Å. Table 2 provides the species, wavelengths, lower excitation potentials, oscillator strengths, and equivalent widths for all five stars and the sun. The log gf values in Table 2 are from the compilations presented in Stephens (1999) and Stephens & Boesgaard (2002).

3.2. Stellar Parameters and Uncertainties

We have used the $(B-V)_0$ values from Hodder et al. (1992) to determine the stellar effective temperature of each star. Although the reddening of 0.28 is high, the good agreement with the values of Zinn (1980) and Geffert & Maintz (2000) suggest that it is rather well-determined. Hodder et al. give errors in B−V of 0.01 for stars in this V magnitude range. We then use the $(B-V)_0$ values to find $T_{\rm eff}$ for both the Carney (1983) (C83) and the King (1993) (K93) temperature scales for metal-poor stars, as we have done in earlier work (e.g. Boesgaard et al. 1998). In addition, we used $(B-V)_0$ and a nominal metallicity of [Fe/H]= −0.70) to find $T_{\rm eff}$ values on the IRFM scale of Alonso et al. 1996); these temperatures agree almost exactly with those on the C83 scale. The uncertainty in the temperatures comes from random errors in the photometry (0.01 mag), the large reddening, and the calibrations. Random errors of $\pm$0.01 mag in both the photometry and reddening estimate both contribute an uncertainty of $\pm$40 K. The two calibrations give $T_{\rm eff}$ values that systematically differ by $\sim$150 K. We carry through the detailed abundance analysis for both sets of temperatures and their associated parameters: log g, [Fe/H], and microturbulence (ξ).

We have used the newest Yale isochrones (Yi et al. 2001) to determine log g values using an age of 12 Gyr, the median of the age values determined by Grundahl, Stetson & Andersen (2002), Salaris & Weiss (1998), and Hodder et al. (1992), for both temperature scales for

metallicities of both −0.70 and −1.30 (and an interpolated value of −1.00). Armed with a set of initial temperatures, consistent theoretical gravities, and a range of overall metallicities, we constructed model atmospheres characterized by these parameters from the grids of Kurucz (1993).

Utilizing an updated (2000) version of the LTE analysis code MOOG (Sneden 1973), we computed absolute Fe abundances from both our Fe I and Fe II equivalent width measurements for an array of trial microturbulence values. For these determinations we used only lines with reduced equivalent width values log (W/λ)≤ -4.82 (generally corresponding to equivalent widths $\leq 75-80$ mÅ). For a given log g and [Fe/H], we determined the combination of $T_{\rm eff}$ and ξ that resulted in the minimal slopes between Fe abundance and a) lower excitation potential, and b) reduced equivalent width. We also tested the effect of varying log g on the agreement between Fe abundance as derived from Fe I and from Fe II.

We adopted model parameters that are given in Table 3. Although we have carried out the abundance analysis throughout on both temperatures scales, we have a preference for the "cooler" scale. (This preference does not imply a preference for the calibration used by C83 over K93 because the large reddening for M71 makes the $B-V_0$ values are uncertain by about $\pm$0.03.) With the cooler scale: 1) there is better agreement with IRFM temperatures, 2) the slopes for Fe I abundance vs excitation potential are closer to zero with our spectroscopic temperatures, and 3) the match with the new evolutionary tracks of Yi et al. (2001) seems better as the tracks do not reach the high turn-off temperatures of the hot stars on the hotter scale.

3.3. Abundances

We employed the updated LTE MOOG code to determine abundances from all our species. MOOG's abfind routine was used with the measured equivalent widths in Table 2 and the appropriate Kurucz model atmosphere characterized by parameters in Table 3. The final abundances for each species are given in Tables 4 (Fe), 5 (Na and α elements), and 6 (Fe-peak: Ni and Cr, and n-capture: Y and Ba) and are discussed below in section 4. For a few lines of some species of particular interest we had to violate our practice of only using features with log (W/λ)< -4.824 (e.g. λ6141 Ba II), but we stay within that limit for all the stellar and solar lines of Fe I, Fe II, Ti I, and Ti II. Where abundances were determined from lines from two ionization stages for an element, an average was determined by weighting the results by the numbers of lines measured.

Also included in those tables are the results for the sun from our lunar spectrum from

Keck/HIRES. For these abundances we used the Kurucz solar atmosphere and the lines for each species that appear in the last column of Table 2. Because the metallicity of the sun is considerably higher than that of the M71 stars, we could not use exactly the same set of lines for the solar abundance determinations. This means that accurate gf values might play a role in determining accurate normalized abundances [X/H]–an issue which we explore below. However, there are a large number of well-determined solar equivalent widths in the set we used for the stars. The solar abundances also appear in Tables 4, 5, and 6. We have used the solar abundances that we determined from the solar/lunar Keck spectrum for consistency in the analysis. Our results are in good agreement with the compilation of Grevesse & Sauval (1998), usually within 0.05 dex. However, our Ca and Ni abundances are 0.18 and 0.20 dex lower than the respective solar photospheric values of Grevesse & Sauval.

An abundance summary with abundances normalized to Fe is given in Table 7. The σ values here represent the error in the mean.

3.4. Uncertainties in the Abundances

The internal uncertainty, σ_μ, in the mean abundance for each species in the five individual stars and the Sun are given in Tables 4, 5, and 6, along with the number of lines utilized in determining the mean abundance; the former come from the line-to-line scatter for each species. For those species where only 1 or 2 lines were used, σ_μ could not be determined. In these cases, a conservative value had to be estimated for later use. In Table 8, internal uncertainties in the mean cluster abundance ratios (column 3) are estimated from the star-to-star scatter of the prenormalized abundances. In column 4 we give the internal uncertainties in the mean abundance ratios that additionally include contributions from the solar values utilized in the abundance normalizations. We note that, for elements with multiple species, all these listed uncertainties include contributions from each species weighted in the same fashion as the mean abundances.

Table 8 also lists the sensitivities of the [Fe/H] and [X/Fe] ratios to the changes in parameter values of T_{eff}, log g, and ξ given above columns 5-7. Typical errors are $\pm$50 K in T_{eff}, $\pm$0.15 in log g, and $\pm$0.15 in ξ. Sensitivities include correlations of errors in element X and Fe. We note that all sensitivities take into account any differences arising from utilizing different ions for a given element. Sensitivity contributions from different species of a given element were weighted in the same fashion as for the mean abundance determinations, i.e. by the number of lines used. Based upon the photometric errors and our parameter investigations, we believe that reasonably conservative estimates of random 1σ-level parameter uncertainties are $\pm$50 K, $\pm$0.15 dex, and $\pm$0.15 km/s in $T_{\rm eff}$, log g,

and ξ, respectively. This means that total uncertainties in the mean abundance ratios are $0.05-0.10$ dex except for [Mg/Fe] and [Ba/Fe]; the latter two ratios have total uncertainties of $\pm$0.12-0.13 dex.

We investigated the effects of our choice of gf values by redetermining abundances for each species utilizing only those specific lines for which solar abundances abundances were also calculated. The abundance differences ("new" minus "old") are given for each star in the fourth row of each species in Table 4 for those species which utilized different line samples for stellar and solar abundance determinations. For example, had we used only those Fe II lines which were also measurable in the Sun, our Fe II-based mean stellar log N(Fe) value would have been 0.060 dex lower. Given the lower weight assigned to the Fe II lines in determining [Fe/H], however, this difference effects our final results negligibly. Indeed, none of our abundances is significantly affected by line sample (and, thus, presumably gf choice) except Na. Table 5 indicates that a truly consistent solar normalization of our Na I lines would have raised our final [Na/Fe] ratio by an additional $\sim$0.08 dex. Whether this systematic change yields a more accurate abundance compared to a value derived from additional lines is, of course, unclear. However, even the difference for this one element is modest.

4. Results

4.1. The M71 Iron Abundance

The abundances for Fe for each star are given in Table 4. For each ion we give the 1σ uncertainty and the number of lines used. The final abundance is the combined result obtained by weights equal to the number of spectral lines that were used for the determination. For Fe we have 79-86 Fe I lines and 8-11 Fe II lines for each star that give the final Fe/H. There are no significant star-to-star variations among the five stars so the mean for the five - the cluster mean - is listed in the final column. Also in Table 4 are the results for the sun from our lunar spectrum with the equivalent widths given in Table 2. We used our solar values, obtained with the same spectrograph, to find [Fe/H].

Our mean M 71 Fe abundance is [Fe/H]= -0.80 ± 0.06 dex, where the uncertainty includes internal uncertainties plus those in the parameters. The final column of Table 4 indicates that our Fe I-based metallicity ([Fe/H]= -0.81) is in excellent accord with the Fe II-based value ([Fe/H]= -0.75) within the internal uncertainties alone (0.03 and 0.07 dex respectively).

For these five turn-off stars we find <[Fe/H]> = -0.80 ±0.02, where the uncertainty

is just the error in the mean. This is in excellent agreement with [Fe/H] = -0.79 ± 0.01 from ten red giant stars in M71 of SKLPS. These comparisons suggest that any intra-cluster dwarf-giant Fe discrepancy is small. This is in contrast to our previous study of the metal-poor globular M92 (King et al. 1998), where we found Fe abundances to be nearly a factor of two smaller in near-turnoff stars than deduced by others in M92 red giants. One possible explanation may be the action of NLTE effects in the near turnoff stars (King et al. 1998). Thévenin & Idiart (1999) have studied NLTE effects on Fe I lines in metal-poor stars. Examination of their Figure 9 suggests that, at the LTE-based Fe abundance of M92 determined by King et al. (1998) (-2.52), NLTE corrections are indeed 0.3 dex. Since these corrections drop to $\sim$0.1 dex at our LTE-based M71 Fe abundance, concordance with previous giant-based determinations is not remarkable. Alternatively, as mentioned by King et al. 1998, it is possible that the M92 dwarf-giant difference is not real or is due to analysis differences. Indeed, Kraft & Ivans (2003) suggest that their analysis of Fe I and Fe II lines in M92 giants indicates the Thévenin & Idiart (1999) NLTE corrections are too large. Kraft & Ivans (2003) conclude that the metallicity of M92 red giants is in the range -2.50 to -2.38, consistent with the earlier estimate of -2.52 by Peterson, Kurucz & Carney (1990) and the King et al. 1998 turnoff results.

The agreement in [Fe/H] between the turn-off stars and the red giants in M71 is a confirmation that high quality spectra and model atmospheres can provide the same benchmark abundance of Fe for this cluster. We can now examine the difference in other element ratios in giant vs. turn-off stars to explore whether nuclear processing and mixing have altered the abundances in the giants.

4.2. Overview of Abundances

The abundances of the other elements are given in Tables 5 and 6 and the mean cluster abundances and parameter sensitivities are given in Tables 7 and 8. Looking at the abundances of the various species in our five M71 stars, there is no firm evidence for genuine star-to-star differences; in particular, no star stands out has having consistently deviant abundances given the uncertainties. Depending on the species, we infer that any genuine star-to-star differences must be at a level of $\leq 0.05 - 0.1$ dex for the particular elements in our sample of stars.

4.2.1. Comparison with Halo Dwarfs of Similar Fe Abundance

Our first comparison is between our M71 stars and field stars of similar metallicity that have been analyzed by Stephens & Boesgaard (2002) (hereafter SB02) because we have used the same line list and the same procedure. There are eight stars in that sample with [Fe/H] between −0.6 and −1.2. The abundances in these eight stars are shown in Table 9. Figure 4 shows the abundances of these Fe-normalized abundances with our mean for M71 as a function of [Fe/H] for four alpha-elements, two Fe-peak elements and two n-capture elements. Compared to the field halo stars, M71 is high in Ca (but would be in the midst of the halo star points at +0.14 had we used the Grevesse & Sauval (1998) solar Ca of 6.36). Although the field stars appear to be low in Ni, which is discussed by SB02, the M71 point would fall among them at −0.10 with the Grevesse & Sauval (1998) solar Ni of 6.25. The field stars are also apparently low in Na (see below).

4.2.2. Comparison with Edvardsson et al. low metallicity disk stars

Edvardsson et al. (1993) (hereafter EAGLNT) derived abundances of 13 elements in some 189 field F and G dwarf stars in the Galactic disk. Several of these stars have [Fe/H] values similar to that of M71. We have separated out those stars with [Fe/H] within ±0.20 dex of −0.80 to compare with our M71 turn-off mean abundances; there are 17 such disk stars and their abundances are given in Table 9. Figure 5 is a similar plot to Figure 4 with the disk stars as filled circles; EAGLNT did not determine [Cr/Fe] so the lower left panel in Figure 5 is [Na/Fe] rather than [Cr/Fe] as in Figure 4.

We can compare Figures 4 and 5 of the abundances in the halo field stars and in the disk dwarfs with our M71 results. Note that although the samples of the disk stars of EAGLNT and those of the halo stars of SB02 have similar metallicities, the orbital characteristics are very different in the two samples. We have examined the U, V, W velocities, the perigalacticon distances, R_p, and the maximum distance above the Galactic plane, Z_{max}, for all the stars in each sample. For example, the |U| values are 4 - 123 km s^{-1} in the disk stars, but 180 - 358 km s^{-1} in the halo stars. With the exception of one disk star, Z_{max} is < 0.85 kpc for the disk stars, while the halo star sample has Z_{max} values are >1.2 kpc, except for one star with low Z_{max} but with |U| = 254 km s^{-1}.

The M71 means for the α-elements appear to match the abundances of the disk dwarfs of comparable metallicity better than they match those of the halo field stars. The value of [Mg/Fe] is at the lower part of the range for both the disk stars and the halo stars, while [Si/Fe], [Ca/Fe], and [Ti/Fe] are somewhat higher in M71 than in the halo stars. According

to Cudworth (1993) the metallicity and U, V, W velocities of M71, −76, −60 and −3 km s^{-1}, are characteristic of the thick disk population.

The abundance of the n-capture element, Ba, in M71 is well-matched by the abundances in the halo stars, but the mean value is more than a factor of two higher than [Ba/Fe] in the disk stars.

4.2.3. Comparison with Sneden et al. M71 Giants

Figure 6 shows the elemental abundances normalized to Fe as a function of atomic number and includes values for our M71 turn-off stars, the ten M71 red giants of SKLPS, and the halo field stars. The giants and turn-off stars agree well in Na and Ni. The alpha-element Ca seems high in the turn-off stars, but would fit perfectly at +0.14 with the Grevesse & Sauval (1998) solar Ca. The alpha-elements Ti and Si are somewhat lower in the turn-off stars than in the giants. Here our Ni abundance is in excellent agreement with the values from the SKLPS giants.

4.2.4. Comparison with Ramírez & Cohen

There are three RC02 M71 stars that are similar to ours in temperature (∼5800 K) and log g (∼4.05) values, which they class as turn-off stars. Although the S/N (per pixel) at 46, 44, 32 for their three stars are somewhat lower than ours for our five stars, their abundances provide a reasonable comparison for our own results. If we determine the mean [Fe/H] from those three stars the same way as we have done for ours, i.e. weighing the results from Fe I and Fe II by the number of lines used, we determine $<$[Fe/H]$>$ = −0.76 ±0.05, which is the same within the errors as our mean of −0.80 ±0.02.

Figure 7 shows the mean abundances normalized to Fe for our five turn-off stars and the three from RC02 along with the abundances of 19 red giants from RC02. One sigma error bars are shown which are the error in the mean. Generally, the abundances agree to within 1-2 σ for the turn-off stars. An exception is [Si/Fe], but although their two stars agree with each other, each has errors of ±0.13 dex. They were only able to measure Cr from one line in one star, so that discrepancy is not important; our Cr abundances come from 16-19 lines of Cr I and Cr II in all five stars. Their Ni abundance is from 2-7 lines in three stars, while ours is from 15-18 lines in five stars. Similarly, we have 21-25 lines of Ti I and Ti II for our Ti abundance in the five stars versus their 4-6 Ti I lines in three stars. Inasmuch as we concentrated on five turn-off stars, we could measure 2-5 times as many lines as they did

for most species, i.e. our turn-off abundances are are based on much more data. However, they examined a large range in stellar luminosity and evolutionary stage and determined abundances of 23 elements, many more than our sample of 10 elements.

It is interesting to compare their results for 19 red giants with those of SKLPS for ten red giants and for their red giants with our turn-off stars. The agreement for the two sets of red giants is good for Na, Si, and Ni. The situation for Ca and Ti seems confusing (see discussion below about alpha-elements). Their red giants seem to be enhanced in Mg and, to a lesser extent, in Na compared to our turn-off-star abundances.

4.3. Fe-Peak Elements

The other two Fe-peak elements, Cr and Ni, are very similar to Fe in our M71 stars. We derive abundances of [Cr/H] of -0.75 ±0.04 from 16-19 Cr I and Cr II lines per star and [Ni/H] -0.71 ±0.04 from 15-18 Ni I lines per star.

The Fe normalized means for the cluster are [Cr/Fe] = $+0.05$ ±0.04 and [Ni/Fe] = $+0.09$ ±0.04. We can compare our results for Ni with those of SKLPS which are based on 3-5 Ni lines in ten giants in M71 (see Figure 6). (They did not measure Cr.) Their value of $<$[Ni/Fe]$>$ = 0.07 ±0.04 (with σ=0.11) is the same as ours to within the errors. The 19 red giants of RC02 have $<$[Ni/Fe]$>$ = $+0.02$ ±0.01 (with σ=0.04) from 13-38 Ni I lines. The similarity of the abundances derived for our turn-off stars and the two sets of giant stars for Ni indicates a constancy between the evolved and unevolved stars. In the case of Cr RC02 find a lower $<$[Cr/Fe]$>$ = -0.13 ±0.01 (with σ=0.06) from 3-10 Cr I lines compared to our $+0.05$ ±0.04 (see Figure 7). (Their [Cr/Fe] for their one turn-off star is still lower at -0.17.) Our [Cr/Fe] ($+0.05$ ±0.04) is the same to within the errors of the halo stars of SB02 ($+0.02$ ±0.02).

4.4. Sodium

We have determined Na abundances in each star from 3-4 Na I lines. These results appear in Table 5. There appear to be no variations from one star to the next. Our mean ratio [Na/Fe] = $+0.14$ ±0.04 agrees well with the $+0.20\pm0.05$ value from RC02 from 3 Na I lines for three turn-off stars just considering our internal uncertainty alone.

Figure 8 shows our M71 results for [Na/Fe] compared to those of the halo field stars of SB02 ($<$[Na/Fe]$>$ = -0.23 ±0.13) and the disk dwarf stars of EAGLNT ($<$[Na/Fe]$>$ = 0.10 ±0.01). The Na content of the M71 turn-off stars is remarkably similar to that of the disk

dwarfs and more than a factor of two higher than that in the halo stars with similar [Fe/H].

Our [Na/Fe] of +0.14 for the turn-off stars has a spread of +0.01 to +0.23, less than half that found in the red giants by both SKLPS and RC02. The spread in our turn-off stars is consistent with the uncertainties in the determinations of [Na/H] for the individual stars and provides no indication of an intrinsic spread. In their study of 10 red giants in M71, SKLPS derived Na abundances from 4 Na I lines which showed a spread in [Na/Fe] from -0.04 to +0.53 and a mean of +0.24 ±0.06 (with σ=0.18). Similarly, RC02 find <[Na/Fe]> = +0.24 ±0.03 (with σ=0.14) and a range of +0.04 to +0.57 in their 19 red giant stars. As can be seen in Figures 6 and 7 there is little difference in the *mean* [Na/Fe] content between the M71 turn-off stars and the M71 red giant stars. However, the sizeable spread in the abundances for individual giant stars indicates that some of the giant stars have Na enhancements, as found in several globular clusters (e.g. in M3 by Kraft et al. 1992, in M13 by Kraft et al. 1993, 1997).

An increased Na could result from the capture of a proton by ^{22}Ne to form ^{23}Na; this could occur in the H-burning shell. The resultant Na is dredged up to the photosphere where it can be observed. An *in situ* processing scenario may or may not be responsible for the cluster's mild O-Na anti-correlation or the range in Na enhancements in the red giants.

Figures 9a and 9b show comparisons of Na with Mg for M71 and the two sets of field stars. Whereas Mg seems similar to the halo stars, the ratio of [Na/Mg] of +0.05 is higher than that in any of the halo or disk field stars. (One can see the M71 point as an extension of the disk-star points toward higher [Na/Mg] at lower [Mg/H]; this is analogous to the trend of [O/Fe] vs. [Fe/H], but with Mg as the chronometer rather than Fe.) For the mean of the 19 red giants, RC02 find [Na/Mg] = −0.12 from an apparent enhancement in Mg in the giants.

4.5. Alpha Elements

We have calculated abundances for four alpha-elements: Mg, Si, Ca, and Ti. For Mg there are only 2-3 lines that we can use for the abundance determination, only 4 for Si, but 18-20 for Ca and 21-25 for Ti. For both Ti and Si we have used lines from neutral and ionized states. The abundances for these α-fusion elements, along with the 1σ uncertainty and the number of lines used in the abundance calculation are presented in Table 5. The Fe-normalized ratios are in Table 7 along with the weighted mean of [α/Fe]. (The weights are the number of lines used in the determination of the abundance of each element.) Again we see no significant star-to-star variations so we have found a cluster average for turn-off stars

for each element, both [α/H] and [α/Fe]. The average alpha-enhancement is [$<\alpha>$/Fe] = +0.29 $\pm$0.05.

Our α-element ratios [Si,Ca,Ti/Fe] show a clear overabundance given the mean values of +0.22, +0.32, and +0.30 with typical total internal uncertainties of 0.05 dex. RC02 find these same ratios from their 2-3 turn-off stars of +0.01, +0.40, and +0.16. For their 19 red giants they find +0.25, +0.43, and +0.21 with uncertainties of typically 0.02 dex. The red giants of SKLPS have those ratios as +0.31, +0.14, and +0.48 with typical uncertainties of 0.04 dex. The straight means for these three α elements are +0.30 (us), +0.19 (RC02 T.O.), +0.29 (RC02 giants), and +0.31 (SKLPS); this is a remarkably consistent alpha enhancement in this cluster in both turn-off and giant stars.

Our mean [Mg/Fe] is +0.09. This is lower than the RC02 value of +0.28 (based on only two turn-off stars they measured) and lower than the RC02 value of +0.37 (based on 19 red giants). It is also lower than the results of Shetrone (1996) who found +0.32 $\pm$0.04 from eight M71 giants. However, our internal uncertainties for Mg are larger than for our other elements.

It is possible that our [Mg/Fe] is in accord with the delayed rise in [Mg/Fe] suggested by Fuhrmann et al. (1995; see their Figure 5) and implies a genuine dwarf-giant difference. Further, the NLTE reanalysis of Galactic Mg ratios by Idiart & Thévenin (2000) suggests there is significant scatter ($\sim$0.6 dex) in [Mg/Fe] at [Fe/H] ~ -0.8. While we have not done the NLTE calculations here, we surmise that our M71 turn-off stars with [Mg/Fe] $\sim$ +0.1 simply lie in the midst of this scatter.

4.6. N-Capture Elements

Table 6 contains the abundance results for our five M71 turn-off stars for Y and Ba based on 3 lines of Y II and 2 of Ba II and Table 7 gives the mean for each element normalized to Fe. We find and [Ba/Fe] = +0.23 $\pm$0.06, [Y/Fe] = +0.15 $\pm$0.05 with [Ba/Y] = +0.08.

Figures 4 and 5 show how our results compare to field stars of similar metallicity in the halo (SB02) and in the disk (EAGLNT). Our M71 stars are quite similar to the halo stars in [Ba/Fe] where the halo mean is +0.16 $\pm$0.01, but a factor of 2 larger than the disk stars where $<$[Ba/Fe]$>$ = $-$0.08 $\pm$0.01. For [Y/Fe] our mean of +0.15 is higher than the value of $-$0.03 found for both the halo stars and the disk stars. These enhancement are modest, and only marginally significant given the uncertainties, but may simply be the consequence of exposure of pre-cluster material to slightly higher neutron flux than that received by most disk field stars. The halo stars have [Ba/Y] = +0.19, while the disk stars [Ba/Y] = $-$0.05

compared to our intermediate value of +0.08. These heavy-to-light ratios, a measure of neutron exposure, are certainly not in conflict with this idea.

The three M71 turn-off stars studied by RC02 have no Y determinations and show a large range in [Ba/Fe]: +0.22, +0.33 and +0.61. The quoted error for the third star is ±0.32; the mean for the other two is +0.27, similar to our [Ba/Fe] of +0.23 ±0.06. Their three evolved stars which do have determinations of [Y/Fe] yield −0.22 while the 25 cluster stars of all evolutionary phases give [Ba/Fe] = +0.34. Their [Ba/Y] of +0.56 is a high value, comparable to those seen in some Ba, S, CH, stars and ω Cen giants. Such large ratios can be produced by very large neutron exposure, which yields significant production of heavy-*s* elements (e.g., Ba) at the expense of light-*s* elements (e.g., Y and Zr) as indicated by both early Clayton et al. (1961) and more recent theoretical calculations (figure 5 of Busso et al. 1995). The expectation from the *s*-process calculations is that the adjacent light-*s* element Zr should show an abundance comparable or just slightly larger than Y, and this is seen in the results of RC02 whose cluster results indicate [Y/Zr]$\sim -$ 0.09. This ratio is unremarkable compared to field stars of similar metallicity (Figure 29 of Edvardsson et al. 1993; Figure 5 of Gratton & Sneden 1994); thus, the RC02 Zr results seem to confirm their Y results.

These heavy elements have been studied in globular clusters and field halo stars by James et al. (2004). For their five field stars with [Fe/H] similar to −0.80 for M71, we find [Ba/Fe] = +0.29, [Y/Fe] = −0.05, and [Ba/Y] = +0.34. The difference is mainly in the low [Y/Fe] values. For the three turn-off stars in the globular cluster 47 Tuc, which has [Fe/H] = −0.69, they find [Ba/Fe] = +0.22, [Y/Fe] = +0.06, and [Ba/Y] = +0.16, values very similar to ours.

We can conclude that the primordial material from which M71 formed underwent at least modestly larger neutron exposure than local field disk stars of similar [Fe/H]. This appears to be true in 47 Tuc as well as deduced from their heavy element abundances in turn-off stars.

The 0.6 dex [Ba/Y] difference between our M71 turn-off stars and the cluster giants of RC02 is surprising, and has potentially significant implications for cluster self-enrichment as manifested by the effects of convective dilution. The reality of this difference needs confirmation by additional observations of light s-peak elements (Y, Rb,Sr, Zr) in M71. In this regard, we note the intriguing circumstance that the mean [Zr/Fe] ratio (-0.23 +/- 0.09) of RC02's 7 most highly evolved stars (log g ¡=1.75) is lower than that (+0.10+/-0.13) of their 3 least-evolved stars (log g¿=2.70) with Zr measurements at the 2.1 sigma level.

4.7. M71 and α Anomalies in the Bulge and Disk

In their study of 10 M71 *giants*, SKLPS noted "normal" 0.2-0.3 dex enhancements of [Si/Fe] and [Ca/Fe]. These match our near-turnoff ratios well. However, they note that their Ti ratio is unusually large: [Ti/Fe]$\sim +0.5$, and call attention to the fact that a similar dichotomy between [Ti,Mg/Fe] and [Si,Ca/Fe] is seen in moderately metal-poor disk and bulge giants (e.g., McWilliam & Rich 1993) *and* in some disk dwarfs EAGLNT. However, both our [Ti/Fe] ratios and those of RC02 do not confirm the larger Ti overabundances noted by SKLPS; rather, they suggest unremarkable values of +0.2 to +0.3 indistinguishable from Si and Ca.

4.8. Self-Enrichment and Pollution Redux

In our previous Keck/HIRES work on M92 (King et al. 1998), we suggested that pollution of these stars' atmospheres along with later *in situ* processing was needed to understand the global picture of this cluster's abundance patterns. Whether such pollution was in the form of abundance variations or previously processed material in the proto-cluster gas or whether it happened after (at least the first generation of?) cluster stars formed (self-enrichment) was not clear. While the idea of such pollution and intra-cluster abundance variations from a *non in situ* source may not be easy to accept, we note additional support for this picture in M92. In their NLTE reanalysis of numerous literature Mg and Ca data, Idiart & Thévenin (2000) include our M92 star equivalent widths. Their Figure 3 contains the striking result that the NLTE [Ca/Fe] abundances in six M92 stars fall nearly precisely along 3 bifurcated sequences defined by field star data. While significant scatter is present for Mg field star data, they suggest a similar trichotomy for the NLTE [Mg/Fe] ratios.

As suggested by Idiart & Thévenin (2000) these intra-cluster differences may indeed be similar to those now well-known in ω Cen, and presumed to arise from self-enrichment from Type II supernovae. Moreover, the correspondence of the M92 star [Ca,Mg/Fe] ratios and the field star sequences may provide renewed support for the idea of globular clusters as the original reservoirs of halo field stars. Regardless, investigating the correspondence of M 71 [Ca,Mg/Fe] ratios and the sequences defined by field stars is clearly important.

However, it is not yet clear that this important task is possible. At [Fe/H]~ -0.8, the field star [Mg,Ca/Fe] sequences in Figure 3 of Idiart & Thévenin (2000) are separated by a modest 0.05-0.1 dex, which is comparable to or smaller than the internal uncertainty in our star-to-star Mg abundances. Moreover, our data need to be subjected to a NLTE analysis in an uniform as possible manner compared to Idiart & Thévenin (2000). At present, we

can only note that there is no strong evidence of intra-cluster [Ca/Fe] differences in M71 from our data; the largest difference seen between our five stars is 0.16 dex, which is a 3σ difference based on the internal star-to-star uncertainties alone; the [Ca/Fe] ratios for the three turn-off stars of RC02 show no evidence of statistically significant bifurcation either. Magnesium abundances of additional little-evolved M71 stars using even higher-quality data would be of great interest in pursuing unsettled questions regarding star-to-star differences perhaps indicative of cluster self-enrichment or primordial abundance variations.

While it was unclear from the work of King et al. (1998) whether any *non in situ* abundance variations in M92 were primordial or the product of cluster self-enrichment, they noted the potential importance of turnoff-giant comparisons in addressing this issue. If self-enrichment occurs after stars have formed, any products that are enhanced (at levels which are easy to detect) in the near turnoff stars may not appear to be enhanced in the red giants. The turn-off stars have relatively thin surface convection zones and the enhancements there may subsequently become unrecognizably diluted as these stars (or stars just slightly more massive) develop deep surface convection zones as they ascend the red giant branch. King et al. (1998) noted that the $\sim$0.5 dex lower abundance for [Mg/Fe] in their M92 near turnoff stars compared to the M92 giants in Shetrone (1996) might indicate the action of self-enrichment in the giants. The difference between the mean M92 near turnoff NLTE [Mg/Fe] ratios from Idiart & Thévenin (2000) and Shetrone's (1996) giant mean remains large at 0.43 dex.

Comparison of intra-cluster dwarf-giant abundances of α-elements is an efficient manner to search for self-enrichment signatures since the production of these is canonically presumed to occur in explosive supernovae having massive (i.e., short-lived) progenitors. We note that, in principle, such stars could also be responsible for r-process contributions to a possible dwarf-giant n-capture difference noted above; while we refer to our heavy elements as "s-process" ones, it must be remembered that such designations are based on *solar system* data. In M71, the RC02 results for Ti and Ca do not provide any evidence for significant near turnoff-giant differences that might be taken as evidence of self-enrichment. Our near-turnoff [Mg/Fe] ratio of $+0.09\pm0.03$ is considerably smaller than the value of the RC02 evolved stars ($+0.39\pm0.014$), which itself should be raised (or ours lowered) by 0.04 dex to account for the modest Fe difference between our studies. While interesting, the meaning of this difference is unclear since the two turn-off stars from RC02 give [Mg/Fe]= $+0.28\pm0.09$, in accord with their giant results. Our turn-off [Si/Fe] ratio is $+0.22\ \pm0.04$, essentially the same as that of RC02 for evolved stars of 0.25 ± 0.03 dex.

We conclude that no α abundance difference is clear between the giants and the turn-off stars. If the n-capture difference noted above is real and resulted from self-enrichment,

then we surmise that polluting material arose in a traditional *s*-process environment–though perhaps one providing an unusually large neutron fluence. We reiterate that mapping any variation of light *s*-element variation with evolutionary status in M71 is critical to determining whether such pollution happened before cluster formation or via self-enrichment after star formation in the cluster.

5. Summary and Conclusions

We have derived abundances of numerous elements in five stars near the turnoff of the relatively metal-rich globular cluster M71 via high-resolution ($R\sim45,000$) spectroscopy with S/N of 50-60 per pixel acquired with Keck/HIRES. Our five stars are very similar to each other in temperature, luminosity, mass, and age. Our derived Fe abundance, [Fe/H]= -0.80 ± 0.06 is in excellent accord with the values measured in both giants and near-turnoff stars by Sneden (1994) and RC02. The lack of a dwarf-giant Fe discrepancy like that we found in the metal-poor cluster M92 may reflect the reduced effects of NLTE on the Fe I abundances in the metal-rich case as suggested by the work of Thévenin & Idiart (1999).

Within our own limited data set, we find no evidence of star-to-star abundance deviations in any element. Furthermore, there are no stars that are consistently higher or lower than the others in the abundances of the various species we studied; among other things, this indicates that our relative temperatures are correct.

We have compared our abundances with two field star samples with metallicities similar to that in M71: eight halo stars from SB02 and 17 disk stars from EAGLNT. Our α-product abundances, Mg, Si, Ca, Ti, seem to fit with both the disk and the halo stars, but perhaps a somewhat better match with the disk stars. (The space motion of M71 is similar to that of disk stars according to Cudworth & Hanson (1993).) For Mg the M71 mean is near the lower edge of both samples. Our M71 mean is more similar in Ni to the disk stars, but Cr matches the halo sample well. Whereas the light s-process element Y is enhanced in M71 relative to both field stars samples, the heavier s-process element Ba is like the halo stars and enhanced more than a factor of 2 above the disk stars.

All the α elements we observed (Mg, Si, Ca, TI) are enhanced relative to Fe as compared to the Sun. The mean enhancement of $<[\alpha/\mathrm{Fe}]>$ is $+0.29\pm0.05$. This is strikingly similar to the mean enhancements in those elements in the red giants in M71 studied by SKLPS and RC02.

It is known that M71 evinces O-Na anticorrelations down to the main-sequence turnoff (RC02) that are presumed to arise from *p*-capture reactions. The totality of data now

available for M71 suggests to us the following two conclusions. First, the similarity of our turn-off Na abundances, as well as those of RC02, with the values observed in M71 giants (SKLPS; RC02) indicates that this p-capture mechanism is not an *in situ* process unless there is a glaring fundamental failure in our basic understanding of stellar structure. The atmospheres of M71 stars must be polluted by material having undergone such processing elsewhere. Second, the lack of clear evidence for intracluster α-element variations suggests that this processing was not the result of self-enrichment via explosive nucleosynthesis – a process which could, in principle, also affect the heavy elements if the r-process came into play. The M71 [Ba/Fe] ratio suggests that material in M71 stars once was present in an s-process environment of at least modestly higher neutron fluence compared to nearby field stars of similar [Fe/H]. It remains unclear whether the s-process polluting source acted prior to cluster formation or after (via self-enrichment). If there is a genuine dwarf-giant Y and/or Zr difference in M71, then it would suggest that a source of modest neutron fluence self-polluted M71 (to produce high light s abundances perhaps seen near the turnoff) in addition to a very high neutron fluence source acting prior to cluster formation (to produce the high heavy-to-light s ratios perhaps seen in the giants). Consistent determination of light s-elements (Rb, Sr, Y, Zr) in a considerably larger sample of M 71 turn-off, subgiant, and giant stars is needed to address this critical issue; the possibility of intra-cluster Mg variations also merits additional study.

Finally, we note the recent work on elemental abundances in the globular clusters M4 ([Fe/H]= -1.08) and M5 ([Fe/H]= -1.21) by Ivans et al. (1999, 2001). Ivans et al. (2001) call attention to the differences in these clusters based upon the morphology of the O-Na anticorrelation patterns and HB morphology. In particular, they note the similarity in the light element processing patterns between M4 and M71, as well as the HB morphology. Indeed, it might be hoped that such an association is a meaningful classification– perhaps related to the dominance of *in situ* processing versus pollution, or perhaps simply related to metallicity since this parameter affects the molecular weight gradient relevant for deep mixing in stellar interiors as well as serving as the "first parameter" controlling HB morphology. The factor of $\geq$2 difference in the M4 and M71 [Ba/Fe] ratios, however, reminds us that the detailed chemical evolution histories of globular clusters are individually unique. As is clear from this investigation, unraveling these histories will require continued study on a star-by-star and cluster-by-cluster basis involving determination of abundances in near turnoff stars via high-resolution spectroscopy on current and future generations of large aperture telescopes.

This work has been supported by an NSF award to AMB, AST-0097955, and the NSF REU program award to the Institute for Astronomy at the University of Hawaii, AST-

9987896. JRK gratefully acknowledges support for this work from NSF awards AST-0086576 and AST-0239518 as well as a generous grant from the Charles F. Curry Foundation to Clemson University.

REFERENCES

Aikawa, M., Fujimoto, M.Y. & Kato, K. 2004, ApJ, 608, 983

Alonso, A., Arribas, S., & Martinez-Roger, C. 1996, A&A, 313, 873

Armosky, B. J., Sneden, C., Langer, G. E., & Kraft, R. P. 1994, AJ, 108, 1364

Boesgaard, A. M., Deliyannis, C. P., Stephens, A., & King, J. R. 1998, ApJ, 493, 206

Boesgaard, A. M. & Stephens, A. 2002, AJ, 123, 1647 (SB02)

Bonifacio, P. 2002, A&A, 395, 515

Bonifacio, P., Pasquini, L., Spite, F., Bragaglia, A., Carretta, E., Castellani, V., Cenutriòn, M., Chieffi, A., et al. 2002, A&A, 390, 91

Briley, M. M. & Cohen, J. G. 2001, AJ, 122, 242

Briley, M. M., Hesser, J. E., Bell, R. A., Bolte, M., & Smith, G. H. 1994, AJ, 108, 2183

Briley, M. M., Hesser, J. E., Bell, R. A., Bolte, M., & Smith, G. H. 1994, AJ, 108, 2183

Briley, M. M., Smith, V. V., Suntzeff, N. B., Lambert, D. L., Bell, R. A., & Hesser, J. E. 1996, Nature, 383, 604

Busso, M., Lambert, D. L., Beglio, L., Gallino, R., Ratteri, C. M., & Smith, V. V. 1995, ApJ, 446, 775

Carney, B. W. 1983, AJ, 88, 623 (C83)

Cavallo, R. M., Sweigart, A. V., & Bell, R. A. 1996, ApJ, 464, L79

Clayton, D. D., Fowler, W. A., Hull, T. E., & Zimmerman, B. A. 1961, Ann. Phys., 12, 331

Cohen, J.G., Behr, B. B. & Briley, M.M. 2001, AJ, 122, 1420

Cohen, J.G. & Meléndez, J. 2005, AJ, 129, 303

Cudworth, K. & Hanson, R.B. 1993, AJ, 105, 168

Denisenkov, P. A., & Denisenkova, S. N. 1990, Soviet Astron. Lett., 16, 275

Edvardsson, B., Andersen, J., Gustafsson, B., Lambert, D. L., Nissen, P. E., & Tomkin, J. 1993, A&A, 275, 101 (EAGLNT)

Fuhrmann, K., Axer, M., & Gehren, T. 1995, A&A, 301, 492

Geffert, M., & Maintz, G. 2000, A&AS, 144, 227

Gratton, R. G., Bonifacio, P., Bragaglia, A., Carretta, E., Castellani, V., Centurion, M., Chieffi, A., Claudi, R., et al. 2001, A&A, 369, 87

Gratton, R. G., & Sneden, C. 1994, A&A, 287, 927

Gratton, R. G., Sneden, C. & Carretta, E. 2004, ARA&A, 42, 385

Grundahl, F., Stetson, P. B., & Andersen, M. I. 2002, A&A, 395, 481

Hodder, P. J. C., Nemec, J. M., Richer, H. B., & Fahlman, G. G. 1992, AJ, 103, 460

Idiart, T. & Thévenin, F. 2000, ApJ, 541, 207

Ivans, I. I., Sneden, C., Kraft, R. P., Suntzeff, N. B., Smith, V. V., Langer, G. E., & Fulbright, J. P. 1999, AJ, 118, 1273

Ivans, I. I., Kraft, R. P., Sneden, C., Smith, G. H., Rich, R. M., & Shetrone, M. 2001, AJ, 122, 1438

James, G., Francois, P., Bonifacio, P., Carretta, E., Gratton, R.G. & Spite, F. 2004, A&A, 427, 825

Kraft, R. P. 1994, PASP, 107, 1773

Kraft, R. P. & Ivans, I. I. 2003, PASP, 115, 143

Kraft, R.P., Sneden, C., Langer, G. E. & Prosser, C.F. 1992, AJ, 104, 645

Kraft, R.P., Sneden, C., Langer, G. E. & Shetrone, M.D. 1993, AJ, 106, 1490

Kraft, R.P., Sneden, C., Smith, G.H., Shetrone, M.D., Langer, G. E. & Pilachowski, C.A. 1997, AJ113, 279

King, J. R., Stephens, A., Boesgaard, A. M., & Deliyannis, C. P. 1998, AJ, 115, 666

King, J. R. 1993, AJ, 106, 1206 (K93)

Kurucz, R. L. 1993, ATLAS9 Stellar Atmosphere Programs and 2 km s^{-1} Grid, CD-ROM 13, (Cambridge, MA: SAO)

Langer, G. E., Hoffman, R., & Sneden, C. 1993, PASP, 105, 301

McWilliam, A., & Rich, R. M. 1994, ApJS, 91, 749

Peterson, R. C., Kurucz, R. L., & Carney, B. W. 1990, AJ, 350, 173

Pilachowski, C. A., Sneden, C., & Wallerstein, G. 1983, ApJS, 52, 241

Pilachowski, C. A., Sneden, C., Kraft, R. P., & Langer, G. E. 1996, AJ, 112, 545

Ramírez, S. V., & Cohen, J. G. 2002, AJ, 123, 3277 (RC02)

Ramírez, S. V., & Cohen, J. G. 2001, AJ, 122, 1429

Salaris, M., & Weiss, A. 1998, A&A, 335, 943

Shetrone, M. D. 1996, AJ, 112, 1517

Sneden, C., Kraft, R. P., Shetrone, M. D., Smith, G. H., Langer, G. E., Prosser, C. F. 1997, AJ, 114, 1964

Sneden, C., Kraft, R. P., Prosser, C. F., & Langer, G. E. 1991, AJ, 102, 2001

Sneden, C., Kraft, R. P., Langer, G. E., Prosser, C. F., & Shetrone, M. D. 1994, AJ, 107, 1773 (SKLPS)

Sneden, C. 1973, ApJ, 184, 839

Spite, F., & Spite, M. 1986, A&A, 163, 140

Stephens, A. 1999, AJ, 117, 1771

Stephens, A. & Boesgaard A.M. 2002, AJ, 124, 2023 (SB02)

Thévenin, F., & Idiart, T. P. 1999, ApJ, 521, 753

Thévenin, F., Charbonnel, C., de Freitas Pacheco, J. A., Idiart, T. P., Jasniewicz, G., de Laverny, P., & Plez, B. 2001, A&A, 373, 905

Timmes, F. X., Woosley, S. E., & Weaver, T. A. 1995, ApJS, 98, 617

Tomkin, J., Lambert, D. L., & Balachandran, S. 1985, ApJ, 290, 289

Ventura, P., D'Antona, F., & Mazzitelli, I. 2002, A&A, 393, 215

Vogt, S. S., Allen, S. L., Bigelow, B. C., Bresee, L., Brown, B., Cantrall, T., Conrad, A., Couture, M., et al. 1994, SPIE, 2198, 362

Yi, S., Demarque, P., Kim, Y.-C., Lee, Y.-W., Ree, C. H., Lejeune, T., & Barnes, S. 2001, ApJS, 136, 417

Yong, D., Grundahl, F., Lambert, D. L., Nissen, P. E., & Shetrone, M. D. 2003, A&A, 402, 985

Zinn, R. 1980, ApJS, 42, 19

This preprint was prepared with the AAS LaTeX macros v5.0.

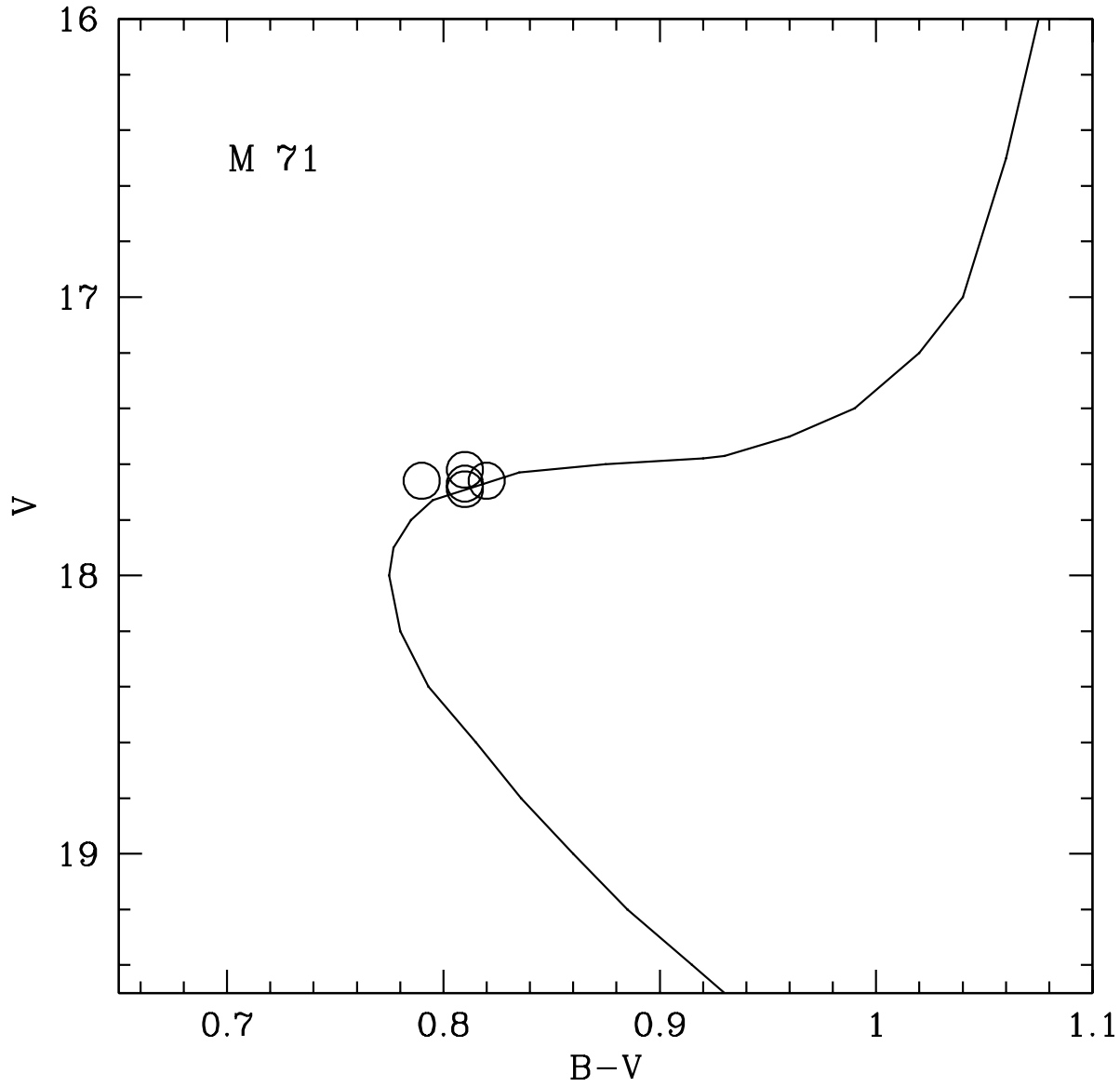

Fig. 1.— The positions of our stars in the color-magnitude diagram. The fiducial sequence is from Hodder et al. (1992). The stars have nearly identical values of V and B-V so have virtually the same temperatures and luminosities as well as masses and ages.

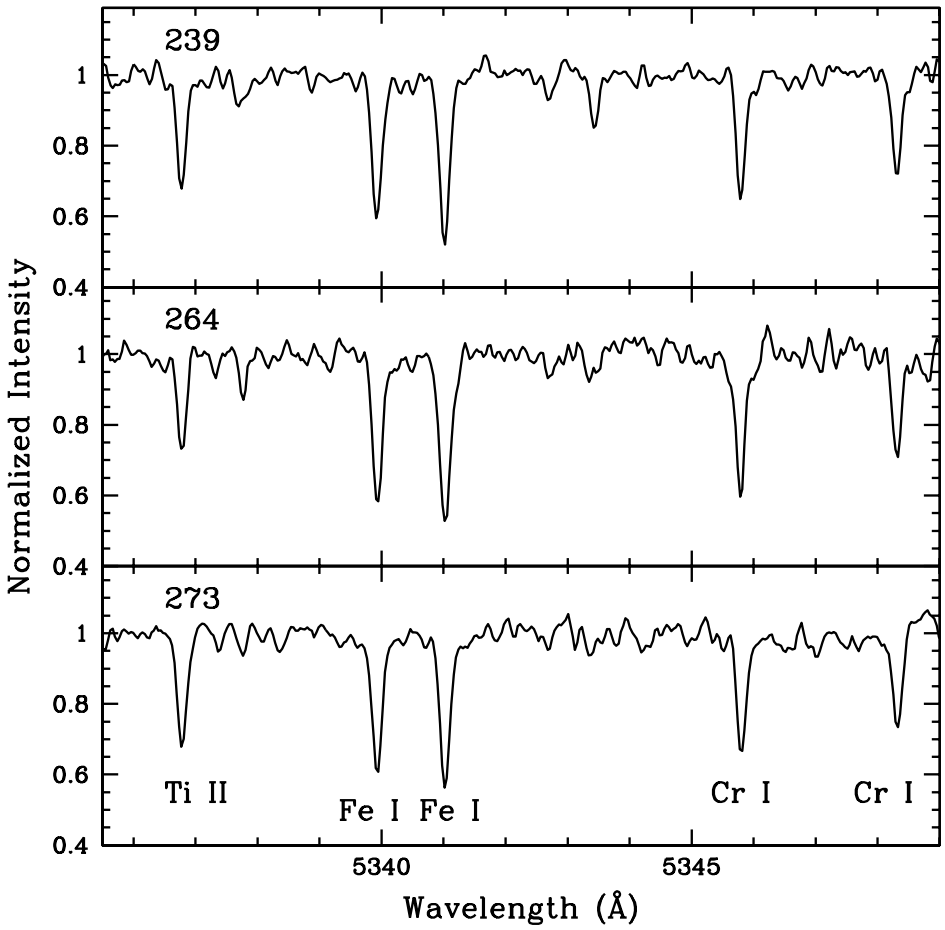

Fig. 2.— Examples of part of one order of the spectra for three of our M71 stars. This sample shows lines due to Fe I, Ti I and Cr I.

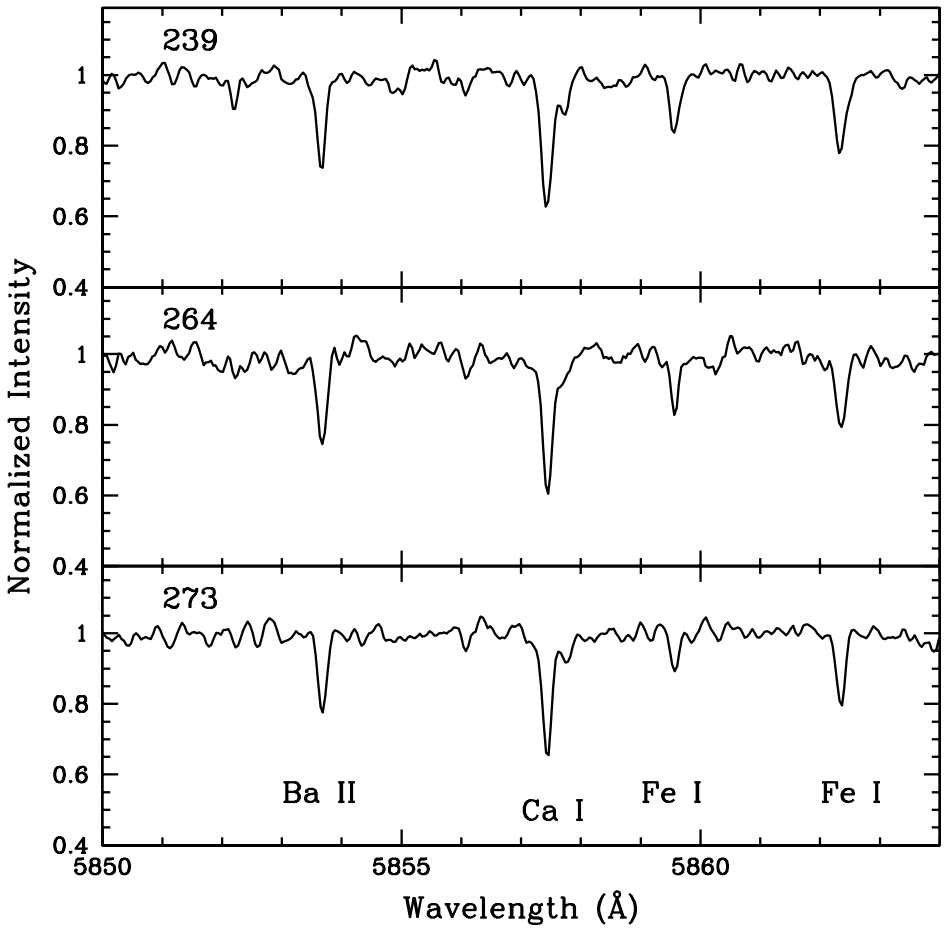

Fig. 3.— Examples of part of another order of the spectra for three of our M71 stars. This sample shows lines due to Fe I, Ba II and Ca I.

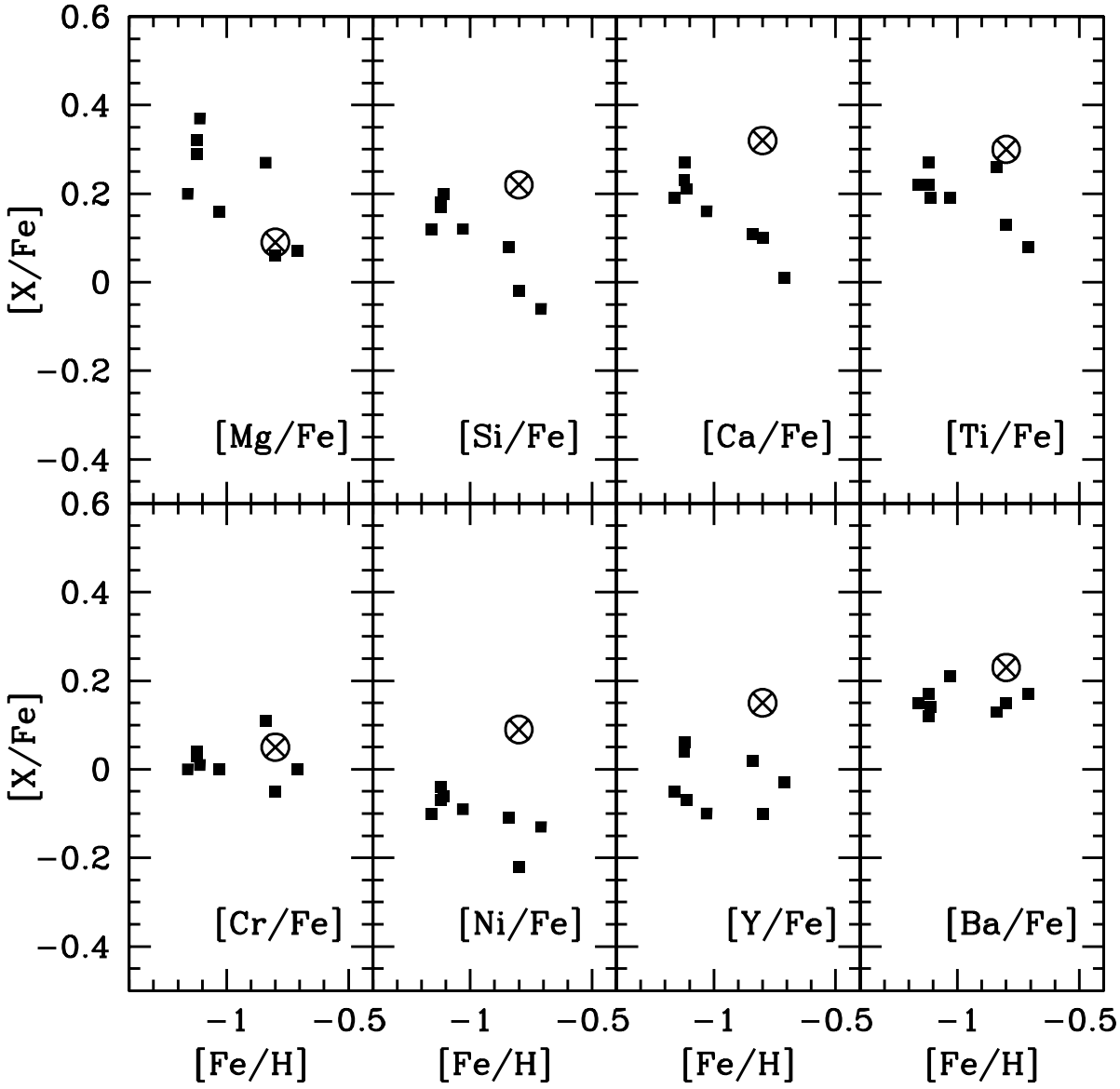

Fig. 4.— Mean Fe-normalized M71 abundances(circled Xs) compared to halo field stars of similar metallicity from SB02 (filled squares).

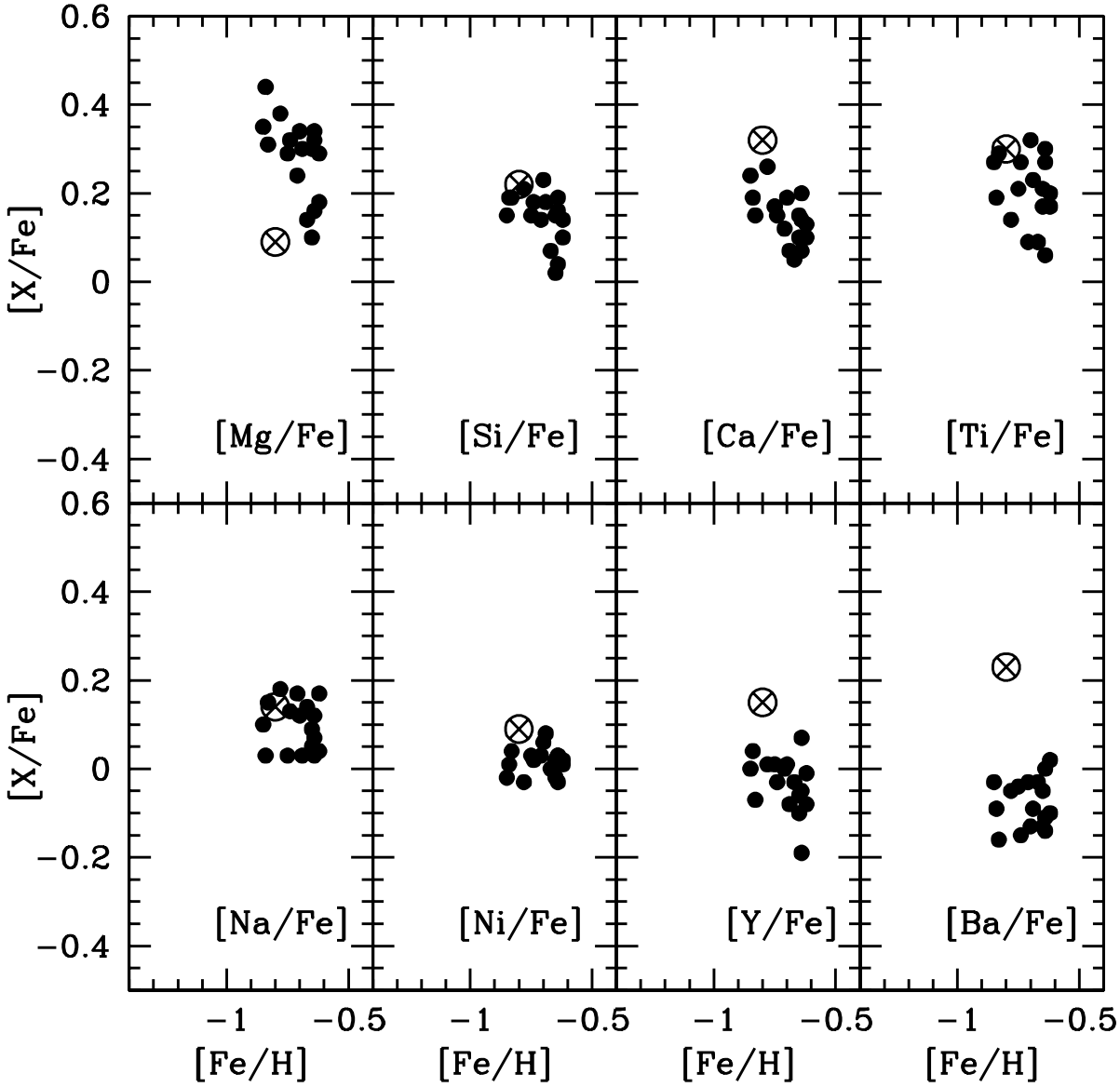

Fig. 5.— Mean Fe-normalized M71 abundances(circled Xs) compared to disk field stars of similar metallicity from EAGLNT (filled circles). This is similar to Figure 4 except that the lower left panel is for [Na/Fe] rather than [Cr/Fe] because EAGLNT did not determine Cr abundances.

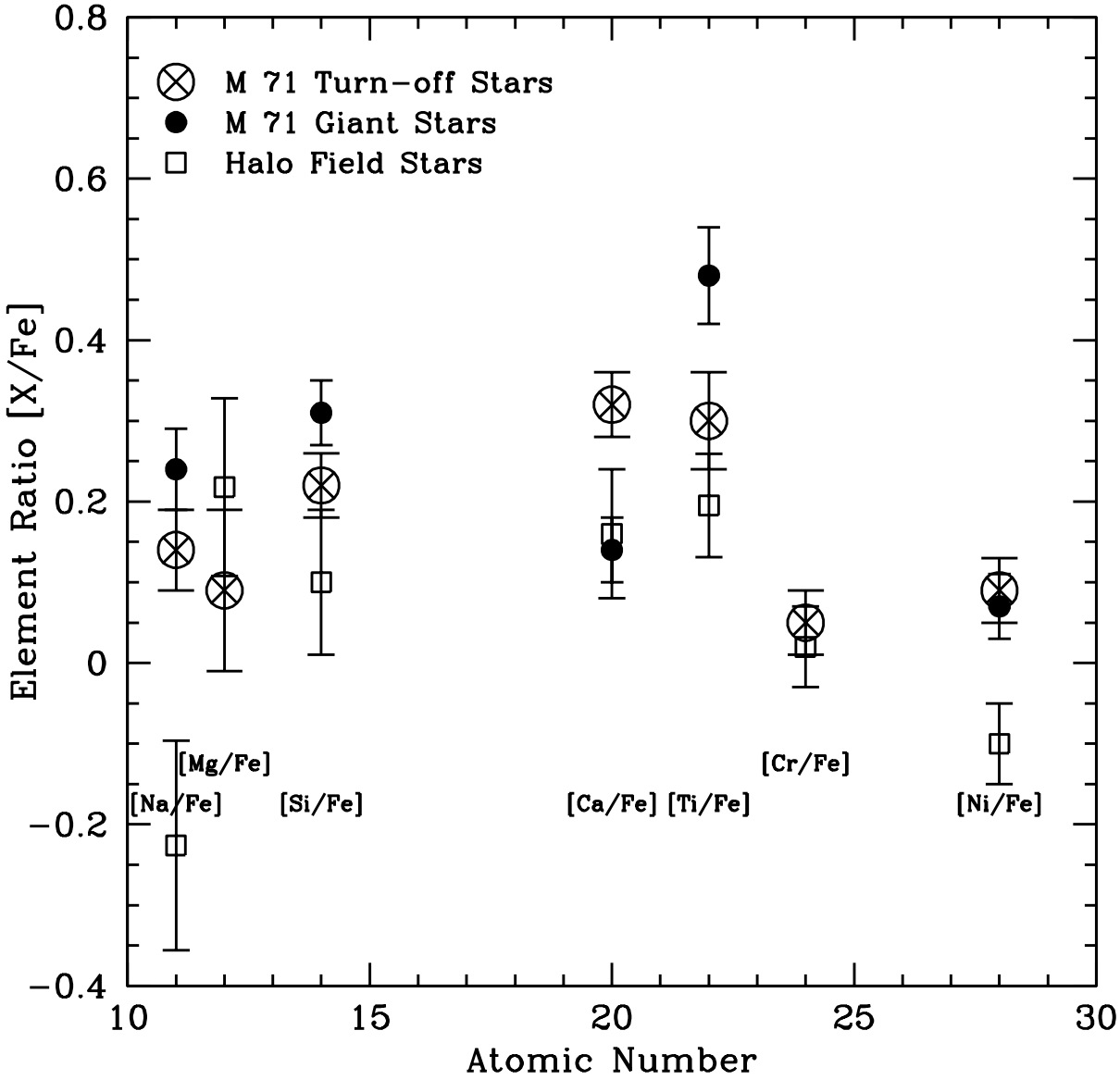

Fig. 6.— Abundance comparisons of our mean abundances for the five M71 turn-off stars with those of SKPLS for ten red giants in M71 and those of SB02 for eight field halo stars of similar [Fe/H] to M71.

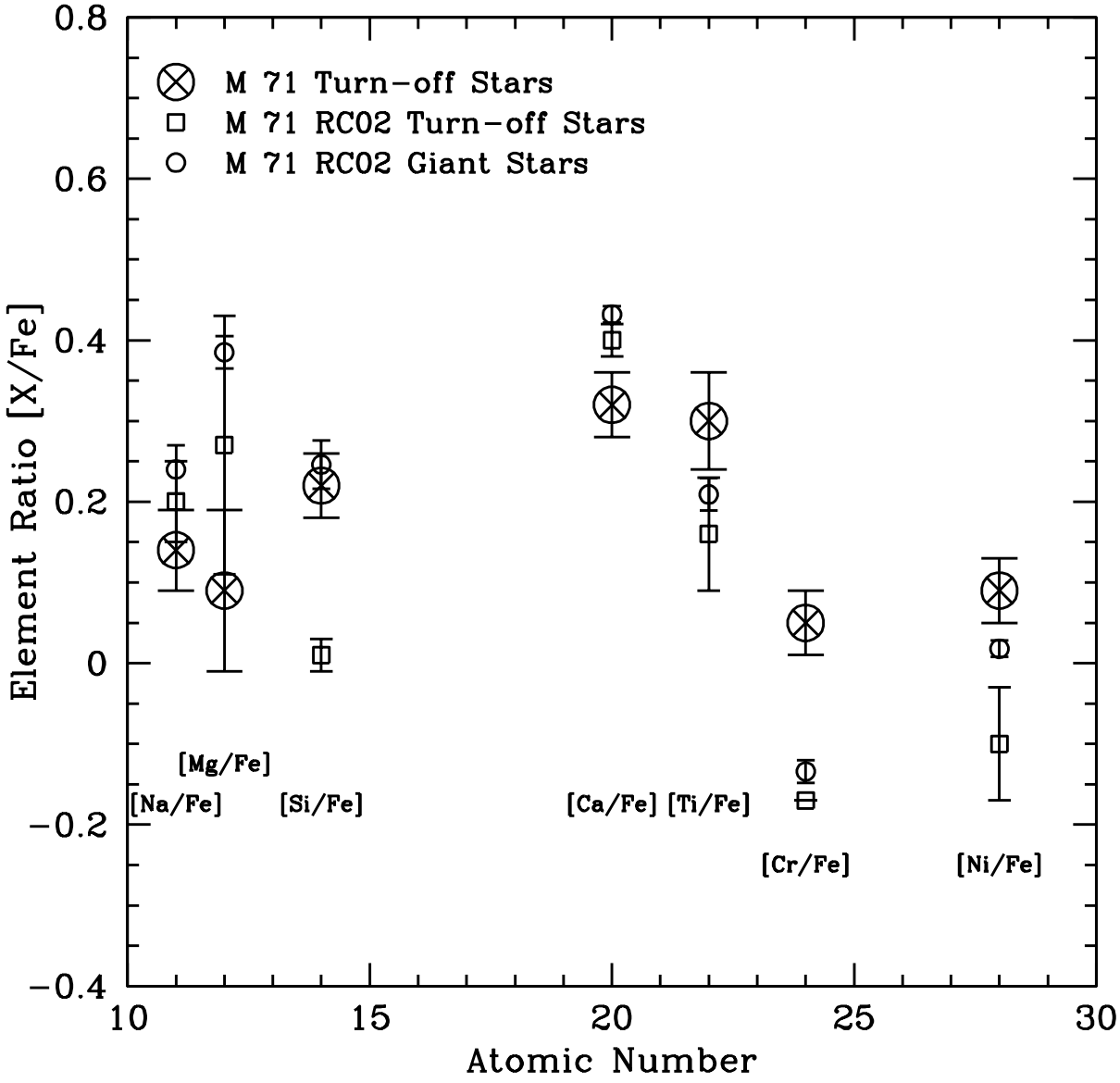

Fig. 7.— Abundance comparisons of our mean abundances for the five M71 turn-off stars with those of RC02 for three turn-off stars and for 19 red giants in M71.

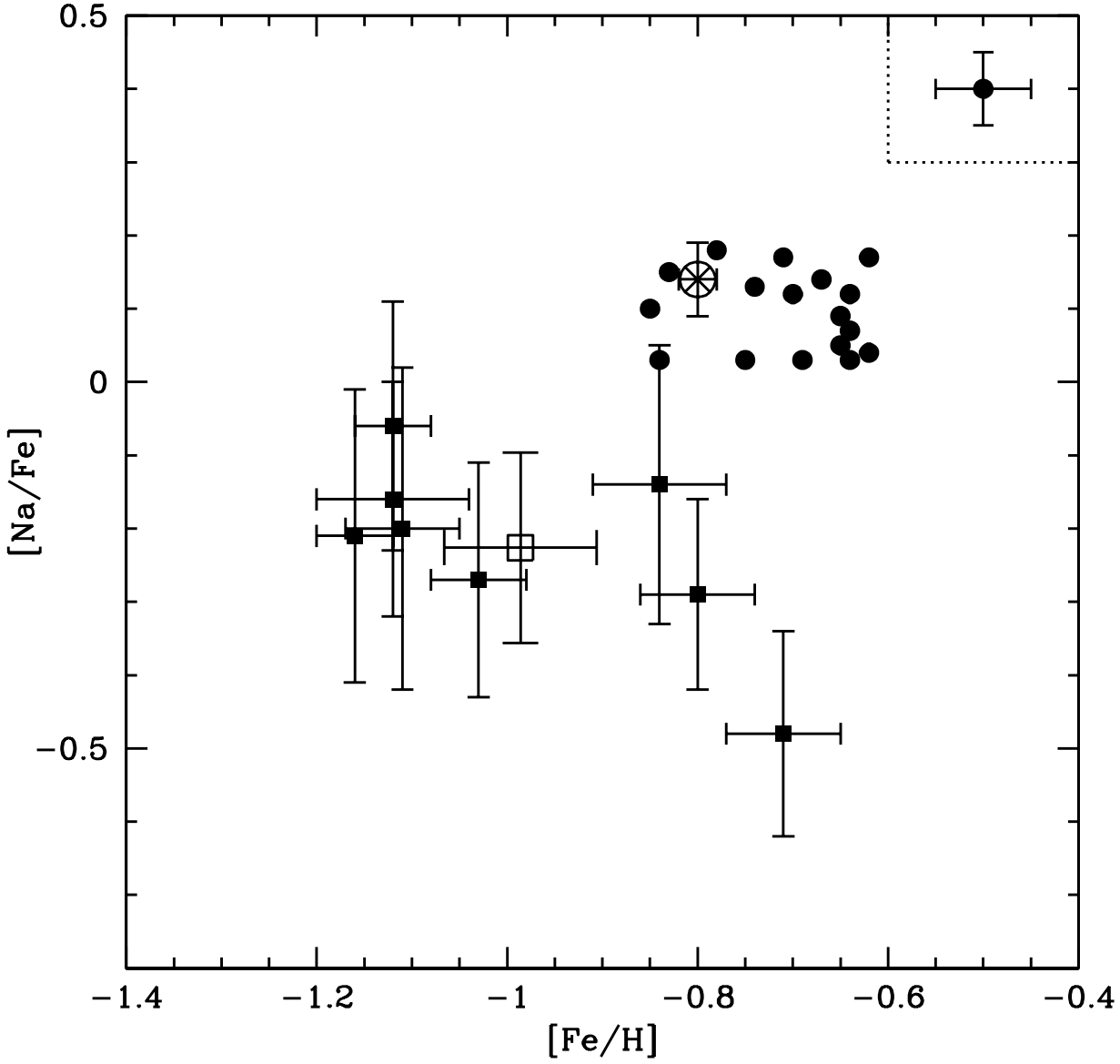

Fig. 8.— Comparisons of [Na/Fe] for the mean of our five M71 turn-off stars with those of EAGLNT for 16 disk stars (filled circles) and of SB02 for eight halo stars (filled squares). The mean for the halo stars is given by the open square. Error bars are shown for M71 and the halo stars, but a typical error bar for the disk stars is shown in the upper right corner.

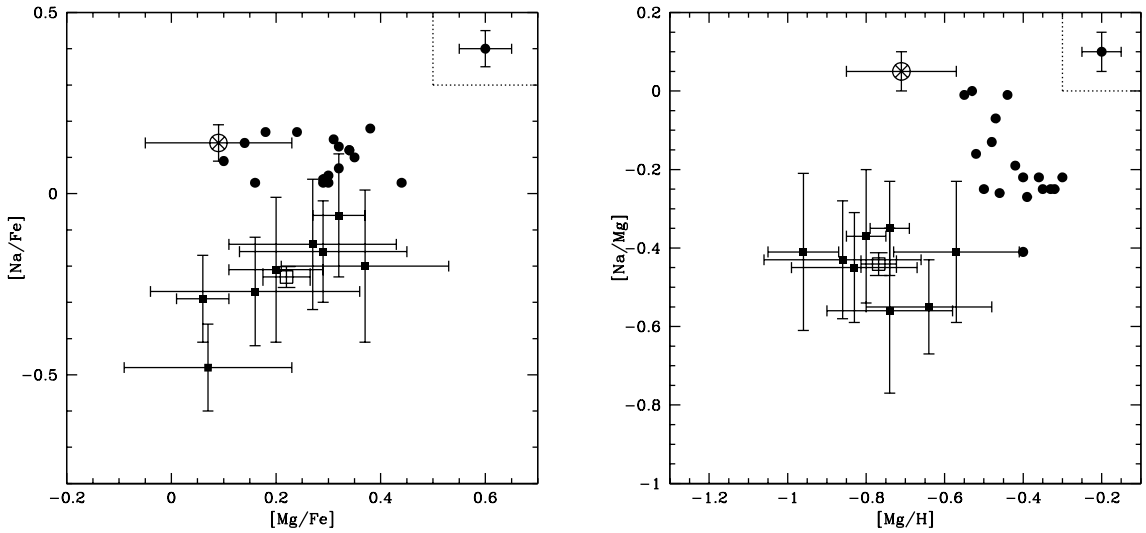

Fig. 9.— Na and Mg abundances. Left panel: [Na/Fe] vs [Mg/Fe] for M71 (circled X), the halo stars of SB02 (filled squares; open square represents the mean) and disk stars of EAGLNT (filled circles). In this comparison M71 appears to be high in Na and low in Mg. Right panel: The [Na/Mg] vs [Mg/H] plot where Mg replaces Fe in Figure 8. M71 has a higher Na/Mg ratio than the disk or halo field stars, but this may simply be the extension of the trend toward higher [Na/Mg] with decreasing [Mg/H] evinced by the disk field stars.

Table 1. M71 Observations

Star	V	B-V	$(B-V)_o$	Night[1]	Total Exp. Time[2] (hr min)	Total S/N
239.....	17.62	0.81	0.53	D, D, F[3], G	3 15	60
259.....	17.66	0.82	0.54	A[3], B, C, C, G	4 00	50
260.....	17.66	0.79	0.51	D, D, G[3]	2 30	50
264.....	17.67	0.81	0.53	D, D, D	2 15	48
273.....	17.68	0.81	0.53	B, C, C, E, F[3], F	4 45	60

[1]A=1996 July 26; B=1996 July 27; C=1997 August 30; D=1997 August 31; E=1998 June 23; F=1998 September 10; G=1998 September 11.

[2]Individual Exposures are 45 minutes, unless otherwise noted.

[3]60-minute exposure.

Table 2. Measured Equivalent Widths

λ (Å)	Ex. Pot. (eV)	$\log gf$	Equivalent Widths 239	259	260	264	273	Sun
Na I								
5682.650	2.1000	−0.8200	40.2	45.6	48.1	38.6	40.1	106.5
5688.219	2.1000	−0.3700	49.5	69.9	63.7	65.4	62.2	···
6154.227	2.1000	−1.6600	7.4	13.9	14.7	···	8.6	37.8
6160.751	2.1000	−1.3500	12.5	···	16.4	27.3	15.5	57.5
Mg I								
4571.099	0.000	−5.5850	71.5	71.5	73.3	63.0	71.3	111.0
4703.98	4.340	−0.5350	160.3	148.6	118.5	149.8	132.9	···
4730.028	4.340	−2.4300	17.7	14.7	···	···	17.5	74.0
6318.72	5.110	−1.6840	···	···	···	···	···	50.8
Si I								
5772.148	5.0809	−1.7500	19.6	30.2	30.2	33.2	15.8	53.0
5948.545	5.0813	−1.2250	54.9	40.0	12.9	42.5	49.0	84.1
6155.141	5.6200	−0.8400	44.0	43.9	37.1	47.0	41.7	83.4
Si II								
6347.100	8.1200	0.3199	28.3	23.0	23.0	29.9	30.7	45.5
Ca I								
4526.934	2.7092	−0.4890	50.0	53.1	42.8	56.8	44.5	···
4578.551	2.5214	−0.6285	49.3	40.7	···	51.6	49.6	···
4685.268	2.9327	−0.8800	32.2	12.1	23.5	···	14.8	···
5188.844	2.9327	−0.0900	···	···	···	···	···	91.1
5260.389	2.5210	−1.8095	13.9	11.1	9.1	10.9	···	···
5261.707	2.5214	−0.6545	62.6	58.0	45.5	60.9	62.1	98.2
5512.980	2.9327	−0.3685	49.7	46.5	47.3	34.9	51.8	86.5
5581.968	2.5232	−0.6325	73.2	55.2	50.3	66.3	66.3	94.4
5590.117	2.5214	−0.6405	56.1	52.1	63.1	63.3	50.8	91.1
5598.480	2.5214	−0.2200	···	···	98.6	···	···	138.4
5601.277	2.5259	−0.6900	69.3	55.8	···	60.5	56.2	···
5857.451	2.9327	0.2350	86.7	80.8	83.0	84.5	69.1	138.4
6163.755	2.5214	−1.2860	31.9	25.5	27.3	33.0	23.7	···
6166.440	2.5214	−1.1400	34.6	37.6	25.3	36.6	23.9	70.3
6169.042	2.5232	−0.7970	59.3	48.0	49.7	58.9	49.0	93.7

Table 2—Continued

λ (Å)	Ex. Pot. (eV)	$\log gf$	Equivalent Widths 239	259	260	264	273	Sun
6169.562	2.5259	−0.3740	60.6	56.4	···	67.8	61.1	112.6
6449.810	2.5214	−0.5020	67.0	68.7	50.5	65.3	52.3	107.8
6455.600	2.5230	−1.3400	30.0	23.2	28.1	24.9	30.0	56.0
6471.661	2.5259	−0.6380	59.2	···	41.7	56.4	···	92.6
6493.781	2.5214	0.0155	87.4	87.2	75.5	98.5	76.8	126.7
6499.650	2.5232	−0.8180	44.0	38.4	33.0	57.6	36.1	86.3
6717.686	2.709	−0.5670	56.2	38.2	59.8	52.8	46.8	···
Ti I								
4518.023	0.8259	−0.2690	48.0	39.7	38.3	40.5	31.7	69.8
4527.305	0.8130	−0.4700	42.2	40.4	40.9	46.4	38.2	···
4534.778	0.8360	0.3360	···	···	71.1	···	···	···
4535.570	0.8259	0.1200	67.7	···	···	69.0	63.0	···
4544.688	0.8182	−0.5200	···	35.2	39.9	···	···	···
4617.254	1.7489	0.4450	25.6	28.1	···	37.2	33.5	60.6
4681.908	0.0480	−1.0150	58.2	38.4	···	51.7	33.0	···
4840.874	0.8996	−0.4530	35.2	40.4	32.8	52.1	24.5	66.4
4999.504	0.8259	0.3060	74.5	66.7	···	···	74.1	···
5016.162	0.8484	−0.5180	42.4	28.1	35.0	29.6	32.2	64.7
5020.028	0.8360	−0.3580	49.1	51.8	36.5	52.4	45.9	78.4
5022.871	0.8259	−0.3780	54.5	49.3	45.8	48.3	35.2	70.1
5035.907	1.4602	0.2600	···	···	59.0	···	···	···
5036.468	1.4432	0.1860	43.7	43.2	53.4	51.5	47.8	74.3
5039.959	0.0211	−1.1300	49.6	49.0	34.2	50.5	42.4	73.2
5064.654	0.0480	−0.8550	58.8	46.1	41.3	62.9	56.0	···
5192.969	0.0211	−0.9500	66.1	54.0	48.0	51.6	···	···
Ti II								
4501.272	1.1156	−0.7550	···	···	···	112.7	···	···
4563.761	1.2214	−0.9600	···	···	···	103.0	···	···
4571.968	1.5719	−0.5300	···	···	···	108.2	···	···
4589.958	1.2369	−1.7900	61.6	70.5	47.1	73.9	54.0	···
4657.203	1.2430	−2.2350	···	36.9	27.1	43.9	43.7	51.4
4779.985	2.0478	−1.3700	50.0	53.3	48.0	56.5	47.4	62.2

Table 2—Continued

λ (Å)	Ex. Pot. (eV)	$\log gf$	Equivalent Widths 239	259	260	264	273	Sun
4805.085	2.0614	−1.1000	63.7	66.4	56.6	80.0	58.1	···
5129.152	1.8918	−1.3900	···	48.5	69.3	73.6	45.8	79.4
5154.070	1.5659	−1.9200	53.7	44.8	43.2	75.3	47.2	72.4
5226.543	1.5659	−1.3000	78.6	81.9	60.9	82.9	73.8	···
5336.781	1.5819	−1.6650	59.4	50.0	54.7	49.6	61.4	71.4
5381.018	1.5658	−2.0250	48.9	45.4	48.4	66.9	46.8	59.6
Cr I								
4496.842	0.9415	−1.1500	···	···	67.3	···	···	···
4540.734	3.1046	0.0280	···	16.6	···	···	···	84.5
4545.945	0.9415	−1.3700	43.7	···	···	···	41.5	84.5
4591.389	0.9685	−1.7400	26.1	···	···	44.9	···	82.6
4600.741	1.0037	−1.2600	46.7	69.3	···	61.6	42.7	92.1
4616.120	0.9829	−1.1900	42.7	55.4	44.1	55.5	45.8	87.6
4626.174	0.9685	−1.3200	48.0	44.4	49.3	44.0	38.9	78.7
4646.148	1.0301	−0.7000	68.9	66.5	···	67.9	···	···
4651.282	0.9829	−1.4600	41.5	44.8	44.8	58.9	31.4	77.0
4652.152	1.0037	−1.0300	55.4	51.8	42.7	64.5	48.8	99.2
4718.426	3.1955	0.0900	···	23.3	···	21.6	···	65.4
5247.566	0.9610	−1.6400	32.0	31.9	32.3	41.8	36.6	81.5
5296.691	0.9829	−1.4000	53.4	42.1	47.0	62.1	46.5	91.9
5298.277	0.9829	−1.1600	···	53.7	63.7	79.7	57.3	···
5345.801	1.0037	−0.9800	62.1	70.4	57.5	70.8	64.3	116.0
5348.312	1.0037	−1.2900	49.8	52.8	41.2	52.9	51.3	100.5
5409.772	1.0301	−0.7150	69.3	85.1	73.5	···	70.4	141.4
6330.093	0.9415	−2.9200	···	···	···	···	···	27.3
Cr II								
4558.650	4.0737	−0.6600	47.2	48.5	44.8	51.7	45.0	78.8
4588.199	4.0715	−0.6300	44.4	49.3	42.0	39.9	41.5	67.9
4634.070	4.0725	−1.2400	···	21.9	26.2	33.3	36.9	61.5
4848.235	3.8647	−1.1400	30.5	40.7	20.1	···	42.6	65.6
5237.329	4.0737	−1.1600	28.3	31.9	33.0	28.4	27.7	51.5

Table 2—Continued

λ (Å)	Ex. Pot. (eV)	$\log gf$	Equivalent Widths 239	259	260	264	273	Sun
Fe I								
4489.739	0.1210	−3.9318	60.4	57.9	50.6	54.8	61.5	···
4556.126	3.6030	−0.7870	61.9	67.8	47.0	61.2	53.3	···
4592.651	1.5580	−2.4556	66.3	···	···	···	···	···
4602.000	1.6080	−3.1439	24.2	27.7	···	···	···	···
4602.941	1.4850	−2.2080	···	···	···	···	···	67.6
4619.287	3.6030	−1.1200	41.4	45.8	38.4	46.9	49.4	···
4625.044	3.2410	−1.3400	45.7	55.6	50.7	55.6	48.2	···
4630.120	2.2790	−2.5935	42.0	···	35.2	44.3	34.1	···
4637.503	3.2830	−1.3900	54.4	38.1	35.7	44.2	48.1	···
4638.010	3.6030	−1.1195	···	33.0	48.7	31.6	42.7	···
4647.434	2.9490	−1.3305	60.7	62.7	46.9	50.6	56.9	···
4669.171	3.6540	−1.3100	···	33.5	22.1	24.1	36.6	···
4678.846	3.6030	−0.7465	53.1	53.6	45.6	57.8	45.4	···
4691.411	2.9910	−1.4865	55.7	···	51.7	53.9	62.6	···
4710.283	3.0180	−1.6120	56.6	53.9	47.0	60.4	50.0	···
4728.546	3.6540	−1.1710	38.2	27.6	39.2	51.5	27.8	···
4733.591	1.4850	−2.9872	47.3	46.1	59.8	54.8	50.1	···
4736.773	3.2110	−0.7460	67.9	···	62.0	70.2	69.9	···
4741.529	2.8320	−1.8820	28.8	30.8	30.0	43.1	31.5	71.4
4882.144	3.4170	−1.6400	35.1	32.7	···	···	27.3	73.6
4924.770	2.2790	−2.2305	38.5	53.9	31.6	35.1	37.7	···
4938.814	2.8760	−1.0770	73.8	···	66.3	···	64.6	···
4939.687	0.8590	−3.3152	···	55.4	50.9	72.4	60.3	···
4946.385	3.3690	−1.1700	58.9	51.0	45.2	68.9	53.6	···
4985.253	3.9290	−0.5590	42.8	44.8	41.1	43.6	59.1	···
4985.547	2.8650	−1.3310	59.7	58.7	46.6	57.5	50.9	···
4994.130	0.9150	−2.9690	68.0	···	59.1	···	68.3	···
5001.862	3.8820	0.0100	···	···	···	···	70.5	···
5022.236	3.9840	−0.5300	···	52.7	50.6	70.6	57.1	···
5028.127	3.5730	−1.1220	47.5	41.6	39.1	···	48.5	···
5044.212	2.8510	−2.0590	38.4	34.8	23.6	35.8	30.9	70.7

Table 2—Continued

λ (Å)	Ex. Pot. (eV)	$\log gf$	Equivalent Widths 239	259	260	264	273	Sun
5049.819	2.2790	−1.3495	···	···	78.1	···	···	···
5051.635	0.9150	−2.7640	···	···	76.6	···	···	···
5068.766	2.9400	−1.1355	70.6	···	64.1	···	72.5	···
5079.224	2.1980	−2.0860	70.6	63.2	52.2	57.8	61.8	···
5079.740	0.9900	−3.2328	68.2	75.6	53.7	···	50.2	···
5083.339	0.9580	−2.8419	74.2	73.1	65.4	···	65.0	···
5110.413	0.0000	−3.7595	···	···	79.7	···	···	···
5123.720	1.0110	−3.0630	70.1	75.6	···	67.8	62.3	···
5150.840	0.9900	−3.0200	···	73.6	54.3	62.1	63.2	···
5151.911	1.0110	−3.3215	61.3	56.6	42.7	60.2	51.5	···
5198.711	2.2230	−2.1130	56.8	49.4	48.6	48.8	55.4	···
5202.336	2.1760	−1.8545	···	···	78.3	···	78.9	···
5215.182	3.2660	−0.8710	59.8	69.2	56.4	56.7	60.6	···
5216.274	1.6080	−2.1160	···	···	72.7	···	···	···
5217.390	3.2110	−1.1160	56.6	71.3	46.2	55.6	41.9	···
5225.525	0.1100	−4.7696	38.0	37.1	40.3	41.3	34.5	73.5
5242.491	3.6350	−0.9035	49.7	49.9	40.4	56.4	42.6	
5250.210	0.1210	−4.9172	32.7	12.5	22.6	32.3	28.0	68.9
5250.646	2.1980	−2.1150	61.8	62.5	53.5	···	62.0	···
5263.305	3.2660	−0.9245	64.1	74.0	64.6	56.4	60.1	···
5307.361	1.6080	−2.9496	52.3	53.4	45.9	47.1	50.2	···
5332.900	1.5570	−2.8579	54.3	53.5	50.8	70.5	44.7	···
5339.930	3.2660	−0.6800	···	···	80.8	···	79.4	···
5373.698	4.474	−0.8600	···	21.2	15.1	···	···	61.0
5379.573	3.695	−1.4970	31.0	17.3	···	33.6	17.8	59.3
5393.167	3.2410	−0.8125	75.1	68.5	69.4	79.8	72.5	···
5497.516	1.0110	−2.8371	70.9	81.1	62.0	84.0	79.4	···
5501.465	0.9580	−2.9978	77.9	69.6	62.7	75.4	72.1	···
5506.779	0.9900	−2.7929	77.6	79.8	55.8	82.9	74.9	···
5560.207	4.435	−1.1900	···	13.9	···	···	···	···
5569.618	3.4170	−0.5130	71.3	···	···	···	···	50.8
5572.841	3.3970	−0.2925	···	···	82.2	···	···	···

Table 2—Continued

λ (Å)	Ex. Pot. (eV)	$\log gf$	Equivalent Widths 239	259	260	264	273	Sun
5576.090	3.4300	−1.0000	67.0	69.5	37.0	57.5	54.6	···
5658.816	3.3970	−0.8360	76.3	71.1	···	···	74.9	···
5717.835	4.285	−1.1300	17.8	17.8	14.7	17.8	···	62.6
5775.080	4.220	−1.2970	16.4	16.9	···	16.9	···	55.5
6012.204	2.223	−4.0381	···	···	···	···	···	24.2
6016.604	3.547	−1.8200	22.4	14.5	···	15.1	21.4	···
6027.048	4.076	−1.1495	27.6	23.9	15.9	27.8	26.0	63.4
6055.992	4.734	−0.4600	23.2	33.7	27.2	34.3	23.4	72.8
6065.481	2.6090	−1.4700	70.6	69.6	74.6	63.6	70.0	···
6078.999	4.652	−1.1200	···	9.6	···	9.6	···	43.3
6127.904	4.143	−1.3990	17.1	13.1	···	17.6	6.5	49.7
6136.615	2.4530	−1.4050	78.7	78.4	71.0	85.8	82.0	···
6137.691	2.5880	−1.3745	82.0	73.3	81.4	80.3	75.6	···
6151.618	2.176	−3.2990	19.7	11.4	11.2	18.6	···	49.0
6157.725	4.076	−1.2600	28.2	25.5	20.4	27.0	···	62.6
6173.341	2.223	−2.8800	31.6	19.8	31.4	40.4	27.6	68.3
6180.203	2.728	−2.6225	···	···	···	···	···	55.6
6219.280	2.1980	−2.4330	60.9	42.9	43.7	49.2	53.0	89.0
6230.723	2.5590	−1.2785	88.7	84.0	80.4	93.6	84.4	···
6240.645	2.223	−3.2030	···	···	···	···	···	48.0
6246.318	3.6030	−0.8770	64.0	60.6	46.4	58.1	58.7	···
6252.555	2.4040	−1.7270	74.8	70.9	71.5	73.9	72.6	···
6254.257	2.2790	−2.4430	···	56.3	···	···	···	···
6322.684	2.588	−2.4475	···	···	···	···	···	75.3
6335.330	2.1980	−2.2035	63.5	50.5	42.2	62.1	48.1	96.8
6344.148	2.433	−2.9000	17.7	22.4	18.9	22.4	18.6	66.4
6355.029	2.8450	−2.3575	28.3	20.2	25.6	···	16.2	78.1
6380.742	4.187	−1.3875	18.1	13.7	···	15.4	···	51.3
6393.601	2.4330	−1.5760	71.8	68.0	63.4	72.8	76.0	···
6481.869	2.279	−2.9840	24.2	19.4	22.2	26.9	18.6	64.1
6494.980	2.4040	−1.2560	96.1	···	90.7	97.3	88.5	···
6498.940	0.958	−4.6946	···	···	···	···	···	47.1

Table 2—Continued

λ (Å)	Ex. Pot. (eV)	$\log gf$	Equivalent Widths 239	259	260	264	273	Sun
6592.913	2.7280	−1.5365	70.9	73.6	65.4	66.7	59.4	···
6593.868	2.433	−2.3940	52.4	42.3	47.1	51.3	46.2	84.7
6609.109	2.559	−2.6765	26.2	17.7	17.7	17.7	20.7	67.1
6750.152	2.4240	−2.6080	28.9	25.6	···	29.5	30.9	73.7
Fe II								
4508.289	2.8580	−2.3210	63.0	60.3	41.4	65.4	55.2	···
4515.339	2.8440	−2.4800	54.3	69.5	···	74.5	55.2	···
4522.634	2.8440	−2.1100	83.3	···	···	85.1	71.4	···
4576.339	2.8410	−2.9550	51.7	···	43.9	···	42.2	61.4
4583.837	2.8070	−1.9200	85.6	76.3	80.2	75.7	83.3	···
4629.339	2.8070	−2.3700	64.0	52.8	73.1	75.9	58.0	···
4923.927	2.8910	−1.3200	···	···	84.3	···	···	···
5197.576	3.2310	−2.1665	52.7	54.1	48.8	57.4	49.0	78.7
5234.630	3.2210	−2.2100	62.6	51.7	61.3	64.1	51.7	···
5276.002	3.2000	−2.0350	68.0	···	82.1	···	74.8	···
5316.615	3.1520	−2.0200	···	86.5	87.9	···	···	···
5325.560	3.221	−2.0750	···	···	···	···	···	41.7
6149.249	3.890	−2.9300	23.7	25.4	···	···	···	36.6
6247.562	3.890	−2.7240	···	22.3	···	···	···	53.5
6456.391	3.9000	−2.3290	51.6	···	46.0	37.8	50.8	···
Ni I								
4714.408	3.3801	0.2300	67.3	···	63.9	···	63.6	···
4715.757	3.5435	−0.3400	34.4	···	···	49.3	32.7	79.3
4756.510	3.4802	−0.3400	43.8	34.9	40.8	49.8	35.1	80.7
4786.531	3.4198	−0.1700	51.8	41.7	57.7	44.9	43.9	95.4
4829.016	3.5424	−0.3300	30.5	21.9	19.1	30.5	29.2	78.5
4831.169	3.6063	−0.4200	35.8	33.7	36.3	34.3	40.3	72.9
4904.407	3.5424	−0.1700	44.0	54.9	44.8	35.5	42.4	85.5
4937.341	3.6063	−0.3900	30.0	36.5	29.1	40.8	22.4	85.3
5035.357	3.6356	0.2900	53.9	56.8	40.1	65.7	51.8	···
5081.107	3.8476	0.3000	60.9	61.3	53.4	52.6	46.0	95.9
5084.089	3.6787	0.0300	54.8	36.4	47.9	46.5	47.7	89.5

Table 2—Continued

λ (Å)	Ex. Pot. (eV)	$\log gf$	Equivalent Widths 239	259	260	264	273	Sun
5115.389	3.8342	−0.1100	41.6	32.1	37.5	40.6	34.9	74.6
5146.480	3.7060	0.1200	···	44.6	37.2	51.8	···	87.0
5155.762	3.8985	−0.0900	44.8	33.7	27.9	42.0	21.5	75.1
5476.900	1.8263	−0.8900	···	···	89.9	···	96.7	···
5587.853	1.9355	−2.1400	30.2	98.6	···	25.0	···	59.3
6108.107	1.6765	−2.4500	···	···	11.9	···	···	64.7
6482.796	1.9355	−2.6300	11.1	9.2	···	10.8	10.2	41.5
6586.308	1.9509	−2.8100	13.9	11.6	···	···	···	43.3
6643.629	1.6765	−2.3000	50.7	40.6	···	51.6	38.6	···
6767.768	1.8263	−2.1700	47.5	37.4	···	41.2	33.8	···
Y II								
4883.684	1.0821	−0.0100	35.2	40.7	34.1	35.3	34.9	55.5
4900.120	1.0313	−0.1300	44.6	50.2	41.2	41.0	41.6	58.0
5087.416	1.0810	−0.3100	34.1	33.4	28.3	22.8	33.9	43.8
Ba II								
5853.700	0.000	−1.0000	48.3	46.7	53.6	52.7	41.5	63.3
6141.700	0.000	−0.0760	96.5	85.6	85.2	93.4	83.7	116.0

Table 3. Model Parameters

Star	Temperature (K)	log g (dex)	ξ (km s^{-1})	Input [Fe/H] (dex)
239.....	5845 ± 45	4.01	1.00	−0.70
259.....	5800 ± 45	3.98	1.00	−0.70
260.....	5930 ± 45	4.08	1.10	−0.70
264.....	5845 ± 45	4.01	1.00	−0.70
273.....	5845 ± 45	4.01	1.00	−0.70

Table 4. Iron Abundances in M 71

Species	Quantity	239	259	260	264	273	Mean	Sun	<[Fe/H]>
Fe I	Mean	6.73	6.64	6.60	6.71	6.64	6.66	7.47	···
	[Fe I/H]	−0.74	−0.83	−0.87	−0.76	−0.83	−0.81	···	−0.81
	σ_μ	0.016	0.018	0.018	0.026	0.016	0.027	0.019	0.031
	# lines	76	76	77	71	76	···	32	···
	ΔMean$_\odot$	+0.044	−0.047	+0.060	−0.027	−0.008	+0.005	···	···
Fe II	Mean	6.68	6.58	6.57	6.71	6.55	6.62	7.37	···
	[Fe II/H]	−0.69	−0.79	−0.80	−0.66	−0.82	−0.75	···	−0.75
	σ_μ	0.053	0.096	0.118	0.078	0.062	0.037	0.053	0.065
	# lines	11	9	10	8	10	···	6	···
	ΔMean$_\odot$	+0.028	+0.001	−0.081	−0.175	−0.075	−0.060	···	···
Fe I & II	Wted Mean	6.72	6.63	6.59	6.71	6.63	6.66	7.45	···
	[Fe/H]	−0.73	−0.82	−0.86	−0.75	−0.83	−0.80	···	−0.80

Table 5. M 71 Abundances for Na and the α Elements

Species	Quantity	239	259	260	264	273	Mean	Sun	<[X/H]>
Na I	Mean	5.53	5.69	5.75	5.68	5.61	5.66	6.32	−0.66
	σ_μ	0.08	0.14	0.10	0.17	0.06	0.05	0.02	0.05
	# lines	4	3	4	3	4	···	3	···
	ΔMean$_\odot$	+0.067	+0.102	+0.076	+0.100	+0.049	+0.078	···	···
	[Na/H]	−0.79	−0.63	−0.57	−0.64	−0.71	−0.66	···	−0.66
Mg I	Mean	6.90	6.80	6.79	6.78	6.90	6.83	7.54	−0.71
	σ_μ	0.06	0.08	0.42	0.05	0.18	0.03	0.14	0.14
	# lines	3	3	2	2	3	···	3	···
	ΔMean$_\odot$	−0.082	−0.077	+0.390	+0.125	−0.013	+0.069	···	···
	[Mg/H]	−0.64	−0.74	−0.75	−0.76	−0.64	−0.71	···	−0.71
Si I	Mean	7.08	7.06	6.93	7.13	7.00	7.04	7.61	−0.57
	σ_μ	0.06	0.12	0.13	0.13	0.07	0.04	0.03	0.05
	# lines	3	3	3	3	3	···	3	···
Si II	Mean	6.95	6.82	6.76	6.99	7.01	6.91	7.55	−0.64
	σ_μ	···	···	···	···	···	0.06	···	0.07
	# lines	1	1	1	1	1	···	1	···
Si I & II	Wted Mean	7.05	7.00	6.89	7.10	7.00	7.01	7.59	···
	[Si/H]	−0.54	−0.59	−0.70	−0.49	−0.59	−0.58	···	−0.58
Ca I	Mean	5.78	5.62	5.68	5.77	5.63	5.70	6.18	−0.48
	σ_μ	0.03	0.03	0.04	0.03	0.04	0.04	0.03	0.04
	# lines	20	19	18	19	18	···	21	···
	ΔMean$_\odot$	−0.027	+0.018	−0.028	−0.010	+0.004	−0.009	···	···
	[Ca/H]	−0.40	−0.56	−0.50	−0.41	−0.55	−0.48	···	−0.48
Ti I	Mean	4.47	4.28	4.41	4.58	4.28	4.40	4.83	−0.43
	σ_μ	0.03	0.04	0.05	0.04	0.04	0.05	0.03	0.06
	# lines	14	14	13	13	13	···	8	···
	ΔMean$_\odot$	−0.004	+0.037	−0.025	−0.011	−0.023	−0.005	···	···
Ti II	Mean	4.52	4.44	4.36	4.68	4.40	4.48	5.09	−0.61
	σ_μ	0.028	0.058	0.082	0.079	0.041	0.064	0.067	0.086
	# lines	7	9	9	12	9	···	6	···
	ΔMean$_\odot$	+0.012	−0.086	+0.079	+0.034	+0.022	+0.018	···	···
Ti I & II	Wted Mean	4.49	4.34	4.39	4.62	4.33	4.43	4.94	···
	[Ti/H]	−0.45	−0.55	−0.55	−0.32	−0.61	−0.50	···	−0.50

Table 6. M 71 Abundances for Fe-Peak and N-Capture Elements

Species	Quantity	239	259	260	264	273	Mean	Sun	<[X/H]>
Ni I	Mean	5.44	5.30	5.29	5.37	5.29	5.34	6.05	−0.71
	σ_μ	0.04	0.04	0.05	0.04	0.03	0.03	0.03	0.04
	# lines	18	17	15	17	17	···	16	···
	ΔMean$_\odot$	−0.007	−0.012	+0.027	−0.023	−0.018	−0.007	···	
	[Ni/H]	−0.61	−0.75	−0.76	−0.68	−0.76	−0.71	···	−0.71
Cr I	Mean	4.76	4.79	4.80	5.01	4.72	4.81	5.53	−0.72
	σ_μ	0.03	0.04	0.06	0.05	0.03	0.06	0.04	0.07
	# lines	13	14	12	12	12	···	15	···
	ΔMean$_\odot$	+0.003	+0.023	−0.029	−0.026	−0.009	−0.008	···	···
Cr II	Mean	4.79	4.88	4.76	4.89	4.90	4.84	5.73	−0.89
	σ_μ	0.04	0.04	0.11	0.11	0.10	0.03	0.09	0.09
	# lines	4	5	5	4	5	···	5	···
Cr I & II	Wted Mean	4.77	4.81	4.79	4.98	4.78	4.83	5.58	···
	[Cr/H]	−0.81	−0.77	−0.79	−0.60	−0.80	−0.75	···	−0.75
Y II	Mean	1.53	1.60	1.48	1.40	1.51	1.50	2.15	−0.65
	σ_μ	0.11	0.11	0.09	0.10	0.10	0.04	0.05	0.06
	# lines	3	3	3	3	3	···	···	···
	[Y/H]	−0.62	−0.55	−0.67	−0.75	−0.64	−0.65	···	−0.65
Ba II	Mean	1.63	1.49	1.61	1.67	1.47	1.57	2.14	−0.57
	σ_μ	···	···	···	···	···	0.045	···	0.05
	# lines	2	2	2	2	2	···	2	···
	[Ba/H]	−0.51	−0.65	−0.53	−0.47	−0.67	−0.57	···	−0.57

Table 7. Cluster Abundance Summary

Element Ratio	Abundance	σ	# lines/star	Species
[Fe/H]	−0.80	±0.02	79-86	Fe I and Fe II
[Na/Fe]	+0.14	±0.04	3-4	Na I
[Mg/Fe]	+0.09	±0.03	2-3	Mg I
[Si/Fe]	+0.22	±0.04	4	Si I and Si II
[Ca/Fe]	+0.32	±0.04	18-20	Ca I
[Ti/Fe]	+0.30	±0.06	21-25	Ti I and Ti II
[$<\alpha>$/Fe]	+0.29	±0.05	45-52	Mg, Si, Ca, Ti
[Cr/Fe]	+0.05	±0.04	16-19	Cr I and Cr II
[Ni/Fe]	+0.09	±0.03	15-18	Ni I
[Y/Fe]	+0.15	±0.04	3	Y II
[Ba/Fe]	+0.23	±0.04	2	Ba II

Table 8. Mean Cluster Abundances and Parameter Sensitivities

Ratio	Mean	σ_μ(int) dex	σ_μ(int+$\odot$) dex	$\Delta T_{\rm eff}$ $\pm$100 K	$\Delta\log g$ $\pm$0.3 dex	$\Delta\xi$ $\pm$0.2 km/s
[Fe/H]	−0.80	0.025	0.035	$\pm$0.074	$\pm$0.005	$\mp$0.052
[Na/Fe]	+0.14	0.064	0.085	$\mp$0.022	$\mp$0.020	$\pm$0.050
[Mg/Fe]	+0.09	0.028	0.12?	$\pm$0.059	$\mp$0.005	$\pm$0.012
[Si/Fe]	+0.22	0.015	0.046	$\mp$0.053	$\pm$0.006	$\pm$0.038
[Ca/Fe]	+0.32	0.023	0.043	$\mp$0.003	$\mp$0.042	$\pm$0.025
[Ti/Fe]	+0.30	0.032	0.056	$\pm$0.008	$\pm$0.021	$\mp$0.001
[Cr/Fe]	+0.05	0.044	0.068	$\mp$0.004	$\pm$0.016	$\pm$0.015
[Ni/Fe]	+0.09	0.013	0.040	$\pm$0.005	$\mp$0.022	$\pm$0.024
[Y/Fe]	+0.15	0.051	0.076	$\mp$0.047	$\pm$0.101	$\pm$0.006
[Ba/Fe]	+0.23	0.037	0.11?	$\mp$0.021	$\pm$0.035	$\mp$0.028

Table 9. Data on Comparison Stars

Star	[Fe/H]	[Na/Fe]	[Mg/Fe]	[Si/Fe]	[Ca/Fe]	[Ti/Fe]	[Cr/Fe]	[Ni/Fe]	[Y/Fe]	[Ba/Fe]
Stars from SB02										
G33-31	−1.12	−0.16	+0.29	+0.17	+0.27	+0.27	+0.03	−0.04	+0.06	+0.12
G5-19	−1.16	−0.21	+0.20	+0.12	+0.19	+0.22	+0.00	−0.10	−0.05	+0.15
G82-5	−0.71	−0.48	+0.07	−0.06	+0.01	+0.08	+0.00	−0.13	−0.03	+0.17
G9-36	−1.12	−0.06	+0.32	+0.18	+0.23	+0.22	+0.04	−0.07	+0.04	+0.17
G114-42	−1.11	−0.20	+0.37	+0.20	+0.21	+0.19	+0.01	−0.06	−0.07	+0.14
G116-53	−1.03	−0.27	+0.16	+0.12	+0.16	+0.19	+0.00	−0.09	−0.10	+0.21
G121-12	−0.80	−0.29	+0.06	−0.02	+0.10	+0.13	−0.05	−0.22	−0.10	+0.15
G168-42	−0.84	−0.14	+0.27	+0.08	+0.11	+0.26	+0.11	−0.11	+0.02	+0.13
MEAN	−0.99	−0.23	+0.22	+0.10	+0.16	+0.20	+0.02	−0.10	−0.03	+0.16
Stars from EAGLNT										
HR 2883	−0.75	+0.03	+0.29	+0.15	+0.17	+0.21	···	+0.03	+0.01	−0.04
HR 8181	−0.67	+0.14	+0.14	+0.07	+0.05	+0.09	···	+0.00	−0.03	−0.03
HR 3018	−0.78	+0.18	+0.38	+0.21	+0.26	+0.14	···	−0.03	+0.01	−0.05
HR 4657	−0.70	+0.12	+0.34	+0.23	+0.19	+0.32	···	+0.06	+0.01	−0.13
HD 22879	−0.84	+0.03	+0.44	+0.19	+0.19	+0.19	···	+0.01	+0.04	−0.09
HD 25704	−0.85	+0.10	+0.35	+0.15	+0.24	+0.27	···	−0.02	+0.00	−0.03
HD 51929	−0.64	+0.07	+0.32	+0.16	+0.14	+0.27	···	+0.03	−0.05	−0.11
HD 62301	−0.69	+0.03	+0.30	+0.18	+0.07	+0.23	···	+0.08	−0.08	−0.09
HD 78747	−0.64	+0.12	+0.34	+0.19	+0.20	+0.30	···	+0.03	+0.07	+0.00
HD 130551	−0.62	+0.17	+0.18	+0.10	+0.10	+0.20	···	+0.01	−0.01	+0.02
HD 134169	−0.83	+0.15	+0.31	+0.19	+0.15	+0.29	···	+0.04	−0.07	−0.16
HD 148211	−0.65	+0.05	+0.30	+0.15	+0.15	+0.21	···	+0.02	−0.10	−0.13
HD 148816	−0.74	+0.13	+0.32	+0.18	+0.15	+0.27	···	+0.02	−0.03	−0.15
HD 159307	−0.71	+0.17	+0.24	+0.14	+0.12	+0.09	···	+0.03	+0.00	−0.03
HD 210752	−0.64	+0.03	+0.16	+0.04	+0.07	+0.06	···	−0.03	−0.19	−0.14
HD 215257	−0.65	+0.09	+0.10	+0.02	+0.10	+0.17	···	−0.02	−0.06	−0.05
HD 218504	−0.62	+0.04	+0.29	+0.14	+0.13	+0.17	···	+0.02	−0.08	−0.10
MEAN	−0.71	+0.10	+0.28	+0.15	+0.12	+0.20	···	+0.02	−0.03	−0.08